scientific reports

Check for updates

OPEN

Network pharmacology and metabolomics analysis of *Tinospora cordifolia* reveals BACE1 and MAOB as potential therapeutic targets for neuroprotection in Alzheimer's disease

S. Amrutha[1], Chandran S. Abhinand[1], Shubham Sukerndeo Upadhyay[1], Ravishankar Parvaje[2], Thottethodi Subrahmanya Keshava Prasad[1]✉ & Prashant Kumar Modi[1]✉

Tinospora **cordifolia has been used for thousands of years to treat various health conditions, including neurodegenerative diseases. The study aimed to elucidate the mechanism of action and protein targets of *T. cordifolia* in the context of Alzheimer's disease through untargeted metabolomics and network pharmacology. LC–MS/MS analysis resulted in 1186 metabolites, including known bioactive compounds such as liquiritin, Plastoquinone 3, and Shoyuflavone A, to name a few. The network pharmacology analysis highlighted the metabolite-protein interaction with the enrichment of 591 human proteins, including neurotransmitter receptors and other regulatory proteins. Pathway analysis highlighted the enrichment of cAMP, mTOR, MAPK, and PI3K-Akt signaling pathways along with cholinergic, dopaminergic, serotonergic, glutamatergic synapse, and apoptosis. The docking results suggest that *T. cordifolia* metabolites could interact with key Alzheimer's disease targets BACE1 and MAO-B, suggesting its role in neuroprotection. These findings provide insights into the biochemical pathways underlying *T. cordifolia's* therapeutic effects and provides a foundation for future exploration of *T. cordifolia* in the context of translational research.**

Keywords *Tinospora cordifolia*, Medhya rasayana, Untargeted metabolomics, Neuroprotection, Therapeutic targets

Abbreviations

TC	*Tinospora cordifolia*
LC–MS/MS	Liquid chromatography and tandem Mass spectrometry
cAMP	Cyclic Adenosine Monophosphate
mTOR	Mammalian Target Of Rapamycin
MAPK	Mitogen-Activated Protein Kinase
PI3K-Akt	Phosphoinositide-3-Kinase–Protein Kinase B
EMS	Enhanced Mass Spectra
EPI	Enhanced Product Ion
IDA	Information-Dependent Acquisition
CID	Collisionally Induced Dissociation
KEGG	Kyoto Encyclopedia Of Genes And Genomes
DAVID	Database For Annotation, Visualization, And Integrated Discovery
STRINGdb	Search Tool For The Retrieval Of Interacting Genes/Proteins Database

[1]Center for Systems Biology and Molecular Medicine, Yenepoya Research Centre, Yenepoya (Deemed to be University), Mangalore 575018, India. [2]Sushrutha Ayurveda Hospital, Puttur 574201, India. ✉email: keshav@yenepoya.edu.in; prashantmodi@yenepoya.edu.in

SMILES ID	Simplified Molecular Input Line Entry System Identity Document
GPCR	G Protein-Coupled Receptors
CHRM1	Muscarinic Acetylcholine Receptor M1
NTSR1	Neurotensin Receptor Type 1
NPY2R	Neuropeptide Y Receptor Type 2
GSK3B	Glycogen Synthase Kinase-3 Beta
STAT3	Signal Transducer And Activator Of Transcription 3
MAP2K2	Mitogen-Activated Protein Kinase Kinase 2
SRC	Proto-Oncogene Tyrosine-Protein Kinase
EGFR	Epidermal Growth Factor Receptor
PDGFRB	Platelet-derived growth factor receptor beta
FLT4	Vascular Endothelial Growth Factor Receptor 3
Nrf2/HO-1	Nuclear Factor Erythroid 2-Related Factor 2/Heme Oxygenase-1
SAMe	S-Adenosylmethionine
DNA	Deoxyribonucleic Acid
RNA	Ribonucleic Acid
CPT	Cryptotanshinone
I/R	Ischemia/Reperfusion
Ach	Acetylcholine
OGD/R	Oxygen Glucose Deprivation/Re-Oxygenation
HIF-1α/LDHA	Hypoxia-Inducible Factor 1-Alpha/Lactate Dehydrogenase A
Aβ	Amyloid Beta
DMSO	Dimethyl Sulfoxide
PBS	Phosphate Buffered Saline
ROS	Reactive Oxygen Species
SEM	Standard Error of the Mean
PI	Propidium Iodide
FBS	Fetal Bovine Serum
DMEM	Dulbecco's Modified Eagle's Medium
AChE	Acetylcholinesterase
ChAT	Choline Acetyltransferase
MAP2	Microtubule Associated Protein 2
MAO-B	Monoamine oxidase B
BACE 1	Beta-site amyloid precursor protein cleaving enzyme
p-Tau	Phosphorylated Tau
PBST	Phosphate-buffered saline in 0.5% Tween-20
RNA	Ribonucleic acid
cDNA	Complementary deoxyribonucleic acid
qRT-PCR	Quantitative reverse transcription polymerase chain reaction
MST1/2	Mammalian sterile 20-like kinase ½
PKCα	Protein kinase C alpha
GSK3-β	Glycogen synthase kinase 3β
Cdk5	Cyclin dependent kinase 5
JNK	C-Jun N-terminal kinase
ERK1/2	Extracellular signal-regulated kinase 1/2

Plant omics is an emerging field in systems biology, offering significant openings for new discoveries and clinically relevant translational research. Plant-based formulations are gaining increased attention for treating various disorders, supported by growing evidence from studies involving cell lines to animal models.

Ayurveda is an ancient medical system that has been widely practiced in India for a considerable period of time. It focuses on disease management and overall health. Ayurveda utilizes whole extract instead of purified compound, leading to a combinatory therapy strategy that maximizes outcomes through mutual efficacy and reduces off-target toxicity through synergistic potency. However, the recurrent use of this medicine faces challenges due to its composition and multi-target mode of action, which needs scientific validation[1].

Metabolomics and network pharmacology-based approaches have been widely used in research to comprehend traditional Ayurvedic herb's medicinal potential better. By combining these techniques, scientists can determine how synergistic compounds found in Ayurvedic medicines engage with target-disease networks, providing new perspectives on the medicinal effectiveness of these plants. This combination of metabolomics and network pharmacology has successfully revealed the modes of action of both complex traditional preparations and medicinal plants[2]. It has also been noted that the principles of Ayurveda combine with systems biology to uncover the routes of active components that could potentially lead to the discovery of new drugs[3].

LC–MS/MS-based studies of medicinal plants, together with network pharmacology, uncover the mechanisms by which several active chemical compounds work together to selectively target and interact with associated proteins or pathways in a synergistic network. The extensive chemical examination by using LC–MS/MS is helpful not only in establishing a connection between complicated chemical mixtures and molecular pharmacology but also in understanding the synergistic effects of combinations, intricate cellular processes, and biochemical pathways through the metabolite-to-gene network[3,4].

Tinospora cordifolia (Thunb.) Miers, also known as Guduchi or Giloy, is a climbing shrub that can be found in India, Sri Lanka, Bangladesh, Myanmar, Indonesia, Malaysia, and Thailand. It is a member of the

Menispermaceae family. In ancient literature, it is known as 'amrita'; it belongs to Medhya Rasayanas, a group of medicinal plants described in Ayurveda to improve memory and intellect[5]. Its medicinal properties are well-reviewed by Upadhyay et al.[6]. Several studies have reported its role as immunomodulatory[7], anti-inflammatory[8], antioxidant[9], hepatoprotective[10], anti-hyperglycemic[11], anti-microbial[12], antihyperlipidemic[13], antipyretic[14], cardioprotective[15], neuroprotective[16], osteoprotective[17], and anti-cancer activities[6,18]. Research has also revealed that *T. cordifolia* enhances memory and learning[19].

T. cordifolia has been well-documented for its beneficial effects on Alzheimer's Disease (AD)[20], including improvements in cognitive decline[21], memory, and learning[22], as well as its ability to manage oxidative stress-related diseases through multiple mechanisms[23].

The plant contains various active compounds, such as alkaloids, glycosides, sesquiterpenoids, phenolics, diterpenoids, steroids, aliphatic compounds, and polysaccharides, responsible for its medicinal properties[6]. It is also a source of micronutrients such as copper, calcium, phosphorus, iron, zinc, and manganese[24].

Although *T. cordifolia* is quite effective, many of its key metabolites, appropriate modes of action, pharmacology, pharmacokinetics, and pharmacovigilance are still not fully understood. *T. cordifolia* exhibits neuroprotective effects, the precise molecular targets within the Alzheimer's disease pathway, including its interactions with amyloid-beta, tau protein, and relevant signaling pathways, require further investigation. Although *T. cordifolia* has demonstrated therapeutic potential in Alzheimer's Disease (AD), its direct interaction with specific enzymes, like BACE1 and MAO-B, has not been previously investigated. While cognitive decline is a primary concern in AD, *T. cordifolia* 's potential impact on other AD-related pathologies, including neuroinflammation, oxidative stress, and neurodegeneration, requires further exploration. As an emerging field, bioinformatics offers valuable tools to facilitate research and accelerate the translation of findings into clinical applications.

In the current study, we used untargeted metabolomics, network pharmacology, and molecular docking approaches to elucidate the molecular correlates of the traditional herb *T. cordifolia* and enable the coverage of many unreported metabolites using LC–MS/MS. We further identified protein targets associated with metabolites of *T. cordifolia* to better understand its complex pharmacological effects. The present study contributes valuable insights into Alzheimer's disease pathology, but further research is necessary to translate these findings into clinically relevant interventions for human use. This finding paves the way for more translational clinical research.

Materials and methods

Materials

Sodium carbonate (Cat# S7795), gallic acid (Cat# 398,225), potassium acetate (Cat# P1190), aluminum chloride (AlCl3), ethanol (Cat# 1.07017), methanol (Cat# 179,337), quercetin (Cat# PHR1488), collagen (Cat# C9791), bisBenzimide H33342 (HOECHST, Cat# B2261), 2′,7′-dichlorodihydrofluorescein diacetate (DCFDA, Cat# D6883), propidium iodide (Cat# 537,059), retinoic acid (Cat# R2625) and primers (Supplementary Table 13) were purchased from Sigma-Aldrich Ltd. U.S.A. Amyloid beta peptide ($A\beta_{42}$) was procured from rpeptide USA (Cat# A-1163–2). Folin-Ciocalteu reagent (Cat# RM10822), 3-(4,5-dimethylthiazol-2-yl)-2,5-diphenyltetrazolium bromide salt (MTT, Cat# MB186), and dimethyl sulfoxide (DMSO, Cat# PCT1303) were purchased from HiMedia Laboratories (India). Fetal bovine serum (FBS, Cat# 10270106), Dulbecco's modified eagle's medium (DMEM, Cat# 12100046) with high glucose, antibiotic and antimycotic solution (Cat#15240062), and trypsin–EDTA solution (Cat# 25200072) were purchased from Gibco, Thermo Fisher Scientific Inc, USA. Antibodies such as BACE1 (D10E5) Rabbit mAb (Cat#5606) and Phospho-Tau (Thr231) antibody (Cat#71429) were obtained from Cell Signaling Technology (Danvers, USA). The Pierce BCA protein assay kit (Cat# 23225) and TRIzol™ Reagent (Cat# 15596026) were obtained from Thermo Fisher Scientific, USA. The cDNA Synthesis Kit (Cat# RR037A) and TB Green Premix Ex Taq II SYBR green master mix (Cat# RR820A) were procured from TAKARA BIOINC, Japan.

Procurement of *Tinospora cordifolia* powder

The study used processed powdered *Tinospora cordifolia* stem (Lot No. 235). It was obtained from the SDP Remedies and Research Centre in Puttur, India, an Ayurvedic drug manufacturer complying with Good Manufacturing Practices (GMP). The industrial processing to obtain *T. cordifolia* powder includes briefly the whole plant of *T. cordifolia*, which was collected and authenticated using macroscopic and microscopic methods by Dr. Harikrishna Panaje, SDP Remedies and Research Centre. A specimen of the same is maintained at the center (*T. cordifolia* ID: SDP/TC/005–2019). The stem of *T. cordifolia* was taken and washed, air-dried under a shade net, vacuum-drum-dried, and then pulverized and sieved to get a fine powder with a yield of 85%. This powder was further used for subsequent experiments.

Quantitative analysis of secondary metabolites

Flavonoids

The total Flavonoid content in *T. cordifolia* triple solvent extract was determined using the aluminum chloride method. Different concentrations of the extract (25, 50, 100, 200, 400, 600, 800, 1000 µg/ml) were mixed with a 10% aluminum chloride and a 1 M potassium acetate solution. After 30 min of incubation at room temperature, the absorbance at 440 nm was measured with quercetin as the standard. The flavonoid concentration was calculated with quercetin as a reference standard in the calibration curve[25].

Phenolics

The total phenolic content present in the *T. cordifolia* triple solvent extract was determined by the Bray and Thorpe method[26]. Different concentrations of the triple solvent extract (25, 50, 100, 200, 400, 600, 800, 1000 µg/ml) were taken, and it was made to 1 ml using distilled water, for which 20% Na_2CO_3 was added and vortexed thoroughly.

After two minutes, Folin's reagent was added, vortexed, and incubated for 30 min at room temperature. The absorbance was measured at 750 nm. The total phenolic content was reported in mg/g by comparing the total Phenolic content of the extract with the calibration curve produced from the reference standard Gallic acid.

Extraction of metabolites

For extraction of metabolites, acetonitrile, methanol, and water were mixed in the proportions of 2:2:1, as previously mentioned[27]. After adding 1 ml of the triple solvent mixture to the 50 mg of *T. cordifolia* powder, it was vortexed, sonicated in an ultrasonic water bath for 10 min, and then centrifuged at 12000 g for 15 min at 4 °C. The supernatant was collected in a fresh tube and dried using SpeedVac (Thermo Fisher Scientific, USA); the dried metabolites were dissolved in 250 µl of 0.1% formic acid and proceeded with LC–MS/MS data acquisition and analysis.

LC–MS/MS-based metabolomics analysis

A QTRAP-6500 mass spectrometer (AB SCIEX, USA) was used to acquire metabolomics data, and it interfaced with Analyst software (v1.6.3) and Analyst Device Driver. Using an Agilent Infinity II 1290 chromatography system (Agilent Technologies, INC Santa Clara, CA 95051, USA) with reverse-phase ZORBAX Eclipse plus C18, RRHD column (2.1 × 150 mm, 1.8 microns) sample resolution was performed. Ten microliters of the metabolite extract were injected into the chromatography column, which was then resolved at a flow rate of 0.3 ml/min with a 20-min gradient using solvents A and B (0.1% formic acid in MilliQ water and 0.1% formic acid in 90% acetonitrile respectively). The gradient employed is as follows: t = 0–1 min, 2% B; t = 10–30% B; t = 11–60% B; t = 13–17, 95% B; and t = 17.2–20, 2% B. The enhanced mass spectra (EMS), enhanced product ion (EPI), and information-dependent acquisition (IDA) method, collectively known as the EMS-IDA-EPI method, were used to acquire the data[28,29]. Data were acquired in low mass mode, with a mass range of 50–1000 Da. This scan monitored the top 5 most intense ions in the range and was scanned at the rate of 10,000 Da/s. The five ions with the highest intensity from the EMS (MS1) mode were selected for fragmentation in the EPI (MS/MS) mode. Metabolite data were obtained in both positive and negative polarities.

During mass spectrometry data acquisition, electrospray ionization was used with the operational parameters included a source probe temperature set at 450 °C, a voltage of either 4,500 V or -4,500 V, a curtain gas maintained at 30 psi, an ion source gas pressure of 30 psi, and a declustering potential applied at either 100 V or -100 V. The precursor ions were fragmented using collisionally induced dissociation (CID) with a collision energy of 40 V (or -40 V), a spread of 25 V, and an entrance potential of 10 (or -10 V). The data for *T. cordifolia* were collected in triplicates in both positive and negative modes.

Data processing and analysis

The raw data from QTRAP-6500 was converted to .mzML format using MSConvertGUI on ProteoWizard open-source tool[30]. The MZmine 2.31 open-source framework was used to analyze metabolite data for identification[31]. The following describes the MZmine data analysis processing parameters. An asymmetry factor of 0.001 and smoothening at 500 units were used for baseline correction. At a noise-level cut-off of 1.0E3, mass detection was done in centroid mode. A minimum peak height of 1.0E3 and minimum time span of 2 min with an m/z tolerance of 0.05 Da were used to reconstruct the chromatogram. Local minima search was used to accomplish chromatogram deconvolution, and the isotopic peak grouper algorithm was used to deisotope the peaks. Non-linear modeling and the RANSAC algorithm were used for alignment, while the peak finder algorithm was used for gap-filling. Using PlantCyc and KEGG (www.genome.jp/kegg/compound/[32,33] as the back-end databases, metabolite identification at the MS1 level was performed using MS2Compound tool[34] with 0.05 Da m/z errors and [M + H], [2 M + H], [M + 2H], [M + ACN + H] as the adducts for positive and [M-H], [M-2H], [2 M-H], [M + FA-H] as the adducts for negative modes. We used the MS2Compound tool for the MS2-level identification of metabolites. This tool utilizes .mgf output files from MZmine 2.31 as input to search the relative intensities at the MS2 level. The precursor tolerance for the fragment searches was kept at 0.05 Da, while the fragment tolerance was 0.5 Da. The most intense metabolites were selected based on their average peak areas from the three runs.

Bioinformatics analysis

MetaboAnalyst 5.0[35] and MBROLE (http://csbg.cnb.csic.es/mbrole2/) version 2.0[36] were used to analyze pathway enrichment, chemical classification, cellular location, and roles for metabolites annotated from the PlantCyc and KEGG databases[32,33]. Using the PubChem Identifier Exchange Service (www.pubchem.ncbi.nlm.nih.gov/idexchange/idexchange.cgi), the SMILES IDs of the metabolites were acquired. Using BindingDB (www.bindingdb.org), a database of protein-small molecule interactions based on experimental data, protein targets of the metabolites were identified[37]. The protein targets identification is based on structural similarity between our compound and known targets in the database. The similarity score ranges from 0 to 1, where 1 indicates an exact match, and 0 indicates no similarity. A score of 0.85 or higher suggests there is a high probability that our compound can interact with the target protein. This screening criteria help us avoid potential false positive protein targets. The DAVID gene ID conversion tool (https://david.ncifcrf.gov/conversion.jsp) was used to convert the UniProt IDs of protein targets from BindingDB to gene symbols and classified them according to the source organism of the gene. Gene ontology classification, protein interaction network, and metabolite–protein joint pathway analysis were performed using DAVID, STRINGdb, and Metaboanalyst tools, respectively. We utilized the Reactome pathway database (https://reactome.org/) to identify the pathways and reactions associated with *T. cordifolia* metabolites in humans.

Cell culture and treatment

For the cell culture experiments, Neuroblastoma cells IMR-32 (ATCC® CCL-127™) sourced from the American Type Culture Collection, USA, were chosen. These cells were cultured in Dulbecco's Modified Eagle Medium (DMEM) containing high glucose and L-glutamine, supplemented with 10% fetal bovine serum (FBS) and 1X antibiotic/antimycotic solution. The culture conditions included maintaining the cells at 37 °C with 5% CO_2 in a humified CO_2 incubator.

A seeding density of 3×10^4 cells per well on collagen-coated 6-well plates was used, and differentiation was carried out using 10 µM retinoic acid in DMEM with 2% FBS over a seven-day period. To create an Alzheimer's disease model, the differentiated cells were treated with $A\beta_{42}$ peptides (0.5 µM) for 48 h[38]. The dried *T. cordifolia* triple solvent extract was reconstituted in incomplete media for cell culture treatments.

MTT assay

Cell cytotoxicity of *T. cordifolia* extract was assessed using MTT assay at varying concentrations as previously described[39]. IMR-32 cells were seeded in a 96-well plate at a density of 5000 cells/well for the cytotoxicity assay. The cytotoxicity assessment was carried out using the MTT assay using (3-(4,5-dimethylthiazol-2-yl)-2,5-diphenyltetrazolium bromide salt). The cells were treated with various concentrations of *T. cordifolia* triple solvent extract (50, 100, 250, 500, 1000, 1500, and 2000 µg/ml) for 48 h. MTT dye was added, and the cells were incubated for 4 h. The resultant formazan crystals were dissolved in a 1:1 mixture of ethanol and DMSO, and the resultant colored solution was read at 570 nm, and the background was subtracted at 650 nm. Untreated cells were used as a control. Cell viability of *T. cordifolia* extract treated cells was calculated in comparison to untreated control cells and expressed as percentage viability.

Cell-staining assay

IMR-32 cells were seeded to 1X collagen-coated 6-well plates in a density of 3×10^4 cells per well and were differentiated using 10 µM retinoic acid for seven days. After differentiation, the cells are treated with $A\beta_{42}$ (0.5 µM), $A\beta_{42}$ (0.5 µM) + *T. cordifolia* extract (200 µg/ml), and *T. cordifolia* triple solvent extract alone (200 µg/ml) for 48 h along with the untreated control cells. After 48 h of incubation, the cells were washed with 1X PBS, and staining assays were performed. For ROS assay, the cells were stained with 2′, 7′-dichlorofluorescein diacetate (DCFDA, 25 µM) and HOECHST (5 µg/ml) for 20 min in dark condition as previously described[40].

For the live-dead cell staining assay, the cells were stained with 20 µg/ml of propidium iodide and 5 µg/ml of HOECHST as a counter nuclear stain for 20 min in the dark, as mentioned earlier[40]. The cells were imaged using the ZOE™ Fluorescent Cell Imager (BioRad Laboratories, California, USA) in red (excitation 556 nm & emission 615 nm) and blue (excitation 355 nm & emission 433 nm) channels for live dead assay and green (excitation 480 nm & emission 517 nm) and blue (excitation 355 nm & emission 433 nm) channels for ROS assay. The ImageJ tool, NIH, USA, was used to analyze the images. The experiment was performed in triplicates.

Real-time-polymerase chain reaction analysis

This experiment investigated the potential of *T. cordifolia* to counteract $A\beta_{42}$-induced changes in gene expression related to Alzheimer's disease. IMR32 cells were seeded in 1X collagen-coated 6-well plates at a density of 3×10^4 cells per well. The cells were then differentiated with 10 µM retinoic acid for seven days. Following differentiation, the cells are treated for 48 h with $A\beta_{42}$ (0.5 µM), $A\beta_{42}$ (0.5 µM) + *T. cordifolia* triple solvent extract (200 µg/ml), and *T. cordifolia* triple solvent extract alone (200 µg/ml) along with untreated control cells. After treatment, the cells were washed with 1X PBS and collected by trypsinization. The RNA was extracted using TRIzol™ reagent according to the manufacturer's instructions. The extracted RNA was quantified using a microvolume spectrometer (Colibri, Germany). One µg of RNA was reverse transcribed into cDNA using the Prime Script 1st strand cDNA Synthesis kit (TAKARA BIOINC, Japan). Following the conversion of RNA to cDNA, qPCR was performed by using cDNA, TB green master mix (TB Green® Premix ExTaq II (Tli RNaseHPlus, TAKARA BIOINC, Japan) and specific primers for AChE, MAP2, MAO-B, and ChAT using CFX96 touch real-time PCR detection system (BioRad, Singapore). β-Actin was used as internal control, and the expression of genes was calculated based on the threshold cycle (CT). ΔΔCT determined the relative expression levels after normalization with β-Actin.

Western blotting

In 6-well plates coated with 1X collagen, IMR-32 cells were seeded at 3×10^4 cells per well, and ten µM retinoic acid was used for cell differentiation for seven days. The differentiated cells were treated with $A\beta_{42}$ (0.5 µM), $A\beta_{42}$ (0.5 µM) + *T. cordifolia* (200 µg/ml) cotreatment, and *T. cordifolia* (200 µg/ml) alone for 48 h. Untreated cells were used as a control group. The medium was removed after the treatment period, and the cells were washed using ice-cold 1X PBS. In a lysis buffer comprising 2% sodium dodecyl sulfate (SDS) in 50 mM triethylammonium bicarbonate (TEABC), sodium orthovanadate (1 mM), sodium pyrophosphatase (2.5 mM), and beta-glycerophosphate (1 mM), the cells were scraped and harvested. Using a Q-Sonica (Cole-Parmer, India), the lysates were probe sonicated on ice and heated for 10 min at 95 °C in a dry bath before being centrifuged at 12,000 g for 20 min. The supernatant was collected, and protein quantification was done using a BCA protein estimation assay kit, followed by Immunoblotting was performed[41]. An equal amount of protein from all the conditions was loaded onto polyacrylamide gel (PAGE), resolved electrophoretically, and then transferred to the nitrocellulose membrane. The membranes were blocked with 5% skim milk (cat# GRM1254 HIMEDIA Laboratories, India) in 1X phosphate-buffered saline in 0.5% Tween-20 (PBST) for an hour following the transfer of the proteins to the nitrocellulose membrane. Primary antibodies for beta-site amyloid precursor protein cleaving enzyme 1 (BACE1), phosphorylated tau (p-tau) (Cell Signaling Technology, Inc. USA) were diluted (1:1000) in 3% BSA in 1X PBST, and the membrane was incubated overnight at 4 °C.

Membranes were washed with 1X PBST. The membranes were then incubated with HRP-conjugated secondary antibodies in 3% BSA in 1X PBST (1:5000 dilution) for two hours at room temperature. The immunoreactive proteins were visualized using Pierce Super Signal West Pico and Super Signal West Dura extended duration chemiluminescence substrate from (Thermo Fisher Scientific USA). VILBER Fusion© FX chemiluminescence imaging system was used to develop the immunoreactive bands. Densitometry analysis of band intensity was carried out using ImageJ (NIH) software, normalized using loading control, and fold-change was evaluated with respect to untreated cells.

Molecular docking studies

In this study, it was shown that metabolic pathways substantially associated with Alzheimer's disease were enriched. Therefore, we conducted a molecular docking study to assess its efficacy in targeting specific proteins, including BACE1 and MAO-B, which are crucial in Alzheimer's disease[42,43]. The X-ray crystallographic structures of the target proteins were obtained from the Protein Data Bank (PDB) (BACE1; PDBID: 2ZHV and MAO-B: PDBID: 2V61) and further prepared by removing heteroatoms and non-protein units. The structures of the identified signature metabolites in the *T. cordifolia* plant and known standard inhibitors of the target proteins were retrieved from the PubChem database. In the study, we use 8-(3-chlorostyryl) caffeine (CSC) (Pubchem CID 5353365) and LY2811376 (Pubchem CID 44251605) known standard inhibitors for MAO-B and BACE1 respectively. The ligand preparation module in Discovery Studio 2022 was utilized to prepare the ligand before undergoing molecular docking, which included refining geometric structures, optimizing ring conformers with low energy, and neutralizing charged groups. We employed the LibDock protocol in Discovery Studio 2022 for the molecular docking study. Before executing the LibDock protocol, we determined the active sites for the inhibitor-interacting amino acid residues in the target proteins using the "Define active site" protocol in Discovery Studio 2022. The selection of the potential ligand from the ligand library was based on the LibDock score and the intermolecular interactions between the phytocompound and the target protein. The validation of the docking protocol was done by re-docking of the native ligand against the active site of MAO-B using Discovery Studio 2022. The docked complex was then aligned with the PDB structure using PyMOL to evaluate the reproducibility of the docking protocol by determining the RMSD value.

Statistical analysis

Statistical analysis was performed using GraphPad Prism-8 software, and the results were presented as mean ± SEM based on three independent experiments. One-way ANOVA with the Bonferroni post hoc test was used in the statistical analysis to compare the groups. $p \leq 0.05$ was considered statistically significant.

Results

Secondary metabolites analysis

We use the aluminum chloride method to determine the total flavonoid content in the triple solvent extract of *T. cordifolia*. The results are presented in milligrams of quercetin equivalents per gram of *T. cordifolia* extract (mg/g). They are expressed as mean ± standard error of the mean (SEM) based on triplicate experiments. Our results showed that there was a concentration-dependent increase in flavonoid content in the triple solvent extract of *T. cordifolia* and had the highest total flavonoid content of 51.62 ± 0.84 ($p \leq 0.001$) at 1000 µg/ml concentration among other tested concentrations (Supplementary Fig. 1a).

The total phenolic content in the triple solvent extract of *T. cordifolia* was determined using the Folin-Ciocalteu method. The results are expressed as milligrams of Gallic acid equivalents (GAE) per gram of *T. cordifolia* sample (mg/g). We observed a significant concentration-dependent increase in the total phenolic content in the triple solvent extract of *T. cordifolia*. The phenolic content of triple solvent extract of *T. cordifolia* is found to be 98.04 ± 1.56 ($p \leq 0.001$) at 1000 µg/ml, the highest among other tested concentrations, Supplementary Fig. 1b.

Metabolite identification for *T. cordifolia* extracts

Mass spectrometry-based untargeted metabolomics were used to unravel the molecular cues of *T. cordifolia* using PlantCyc and KEGG databases. The schematic representation of the workflow applied in this study and representative total ion chromatogram from the positive mode is given in Fig. 1a & 1b, respectively. Metabolite identification was performed at the precursor level and fragment levels. The analysis identified 538 (45.4%) and 553 (46.6%) unique metabolites in positive and negative modes, respectively, and 95 (8%) common metabolites, summing to a total of 1186 nonredundant metabolites at the MS1 level (Supplementary Fig. 2a). The detailed list of identified metabolites at the MS1 level from MZmine searched data in positive and negative modes is presented in Supplementary Tables 1 and 2, respectively.

We also identified metabolites at the MS/MS level using our in-house tool, MS2Compound[34]. We identified a total of 516 metabolites at the MS2 level, including 230 (44.6%) and 264 (51.2%) unique metabolites from both positive and negative modes, respectively, and 22 (4.3%) were shared between them (Supplementary Fig. 2b). The complete list of metabolites identified at the MS/MS level in positive and negative modes is given in Supplementary Tables 3 & 4. Table 1 lists the representative top intense metabolites from *T. cordifolia* based on their average peak area of triplicate measurements; their respective intensities and polarities are also listed. Those with the highest average peak area were selected as intense metabolites among all metabolites.

Identification of previously reported metabolites from *T. cordifolia* extract

Our analysis also led to the identification of several previously reported metabolites in *T. cordifolia,* including L-homoserine (121.08 m/z), N-a-Acetyl-L-arginine (217.08 m/z), Hypotaurine (110.04 m/z), 2-Methylbenzenethiol (125.04 m/z), peonidin (345.11 m/z), Cryptotanshinone (341.16 m/z), Deoxyuridine triphosphate (513 m/z), N-cis-Feruloyltyramine (312.11 m/z), (S)-N-Methylcoclaurine (344.16 m/z)

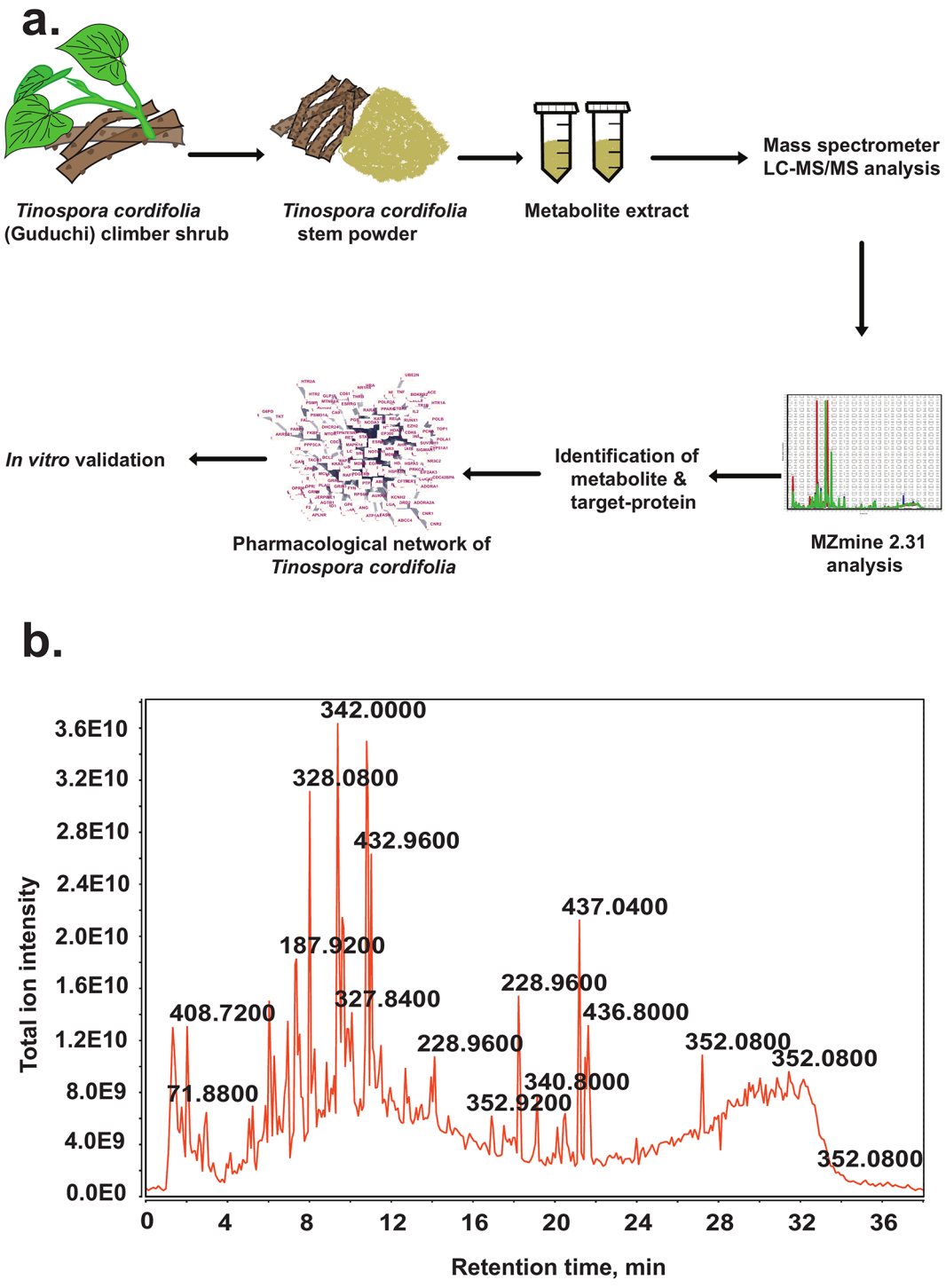

Fig. 1. Illustration of the global untargeted metabolomic analysis of *T. cordifolia*. (**a**) Schematic workflow of metabolite extraction from *T. cordifolia* stem powder, LC–MS/MS analysis using QTRAP-6500 mass spectrometer, followed by metabolite identification using MZmine tool (version 2.31) and subsequent bioinformatics analysis and in vitro validation of neuroprotective activity. (**b**) Representation of total ion chromatogram of *T. cordifolia* metabolite analysis in positive mode. Label: LC–MS/MS, liquid chromatography-tandem mass spectrometry.

and Syringin (371.16 m/z) are present in both precursor and fragment-level in this study, and Oblongine (313.20 m/z), L-arginine (177.12 m/z), O-aminobenzaldehyde (122.04 m/z), (S)-norcoclaurine (136.08 m/z), 5,6-dihydrouracil (227.16 m/z), S-Adenosylmethionine (398.16 m/z), choline (207.24 m/z), Sebacic acid (403.32 m/z), 14-Heptacosanol (791.88 m/z), Isocolumbin (357.12 m/z), Magnoflorine (341.16 m/z), palmatine

m/z, (Da)	Retention time, minutes	Metabolite identification	Peak intensity	Polarity
432.84	10.81	3-(3,5-Diiodo-4-hydroxyphenyl)pyruvate	3.27E + 10	+
414.96	10.81	Perfluorooctanoic acid	3.8E + 10	+
785.88	29.62	1-Cyclohexyl-11-heneicosanone	3.7E + 10	+
605.16	32.05	5,7,3'-Trihydroxy-4'-methoxyflavanone	3.5E + 10	+
757.8	30.67	Erucoylacetone	3.2E + 10	+
352.2	29.02	O-sinapoylcholine	9.21E + 09	+
338.16	32.33	Deoxynivalenol	3.2E + 09	+
542.76	1.36	Cyclolinopeptide F	2.7E + 09	+
271.92	7.36	Di-2-thienyl disulfide	5.13E + 09	+
383.16	9.88	Cassythine	1.4E + 09	+
144.96	7.55	thioacrolein	1.4E + 09	+
183.96	30.07	Arsenate	1.3E + 09	+
339.48	31.88	N-Dodecane	2.1E + 08	-
742.32	30.96	Agavoside F	1.9E + 08	-
309.12	25.54	Ilicifolinoside A	1.4E + 07	-
692.76	16.48	Captafol	2.3E + 07	-
343.2	14.28	corynantheal	2.4E + 07	-
387.12	8.56	Dictyoquinazol C	3.7E + 08	-
175.2	1.01	Putrescine	2.4E + 07	-
293.04	7.98	Wasalexin A	3.2E + 07	-
315.12	6.04	Hypoglycin B	1.1E + 08	-
371.06	15.87	psoralen	3.3E + 07	-
328.08	12.81	Avenanthramide 1p	5.6E + 07	-
369.12	8.44	Linusitamarin	6.2E + 07	-
71.88	1.70	Unassigned	3.4E + 09	+
609.72	11.09	Unassigned	7.8E + 08	+
83.88	1.42	Unassigned	7.6E + 08	+
788.88	30.31	Unassigned	1.4E + 09	+
585.84	13.09	Unassigned	3E + 08	+
83.88	4.10	Unassigned	2.9E + 07	+
682.8	9.38	Unassigned	1.6E + 08	+
788.88	28.31	Unassigned	1.5E + 09	+
338.42	13.50	Unassigned	5E + 07	-
608.82	10.36	Unassigned	1E + 08	-
357.72	9.94	Unassigned	2E + 07	-
326.52	9.13	Unassigned	3E + 07	-
686.88	10.47	Unassigned	2E + 07	-
135.24	1.25	Unassigned	5E + 07	-
413.64	10.95	Unassigned	2E + 07	-
406.44	8.80	Unassigned	1E + 07	-

Table 1. List of Intense Metabolites Identified in *T. cordifolia*.

(175.55 m/z), and berberine (335.16 m/z) are present in precursor level. The representative spectra of some of these signature metabolites are provided in Supplementary Fig. 3 a-d.

Identification of metabolites that are not previously reported from *T. cordifolia* extract

We have also identified several new metabolites not previously identified in *T. cordifolia* extract, including Liquiritin (417.12 m/z), Plastoquinone 3 (339.24 m/z), Poppy acid (201 m/z), Selenomethionine (198 m/z), 11Z-Eicosenoic acid (352.32 m/z), Theaflavin-3-gallate (758.16 m/z), Quercetin 3, 3'-bissulfate (504 m/z) and Shoyuflavone A (194.04 m/z) (Supplementary Fig. 4 a-d). From the intense metabolites, metabolites which were not previously reported, as identified through a literature survey, are presented in Table 2.

Unassigned metabolic features from *T. cordifolia* extract

While we utilized two databases (PlantCyc and KEGG) to match the identified metabolites, a considerable number of intense features in our metabolomics data remained unassigned (127 at the MS1 level and 2248 at the MS2 level), which are actually metabolites. These unidentified metabolite features cannot be overlooked, as they may hold crucial insights into the molecular composition of the formulation, which can be inferred from

m/z, (Da)	Retention time, minutes	Metabolite identification	Peak intensity	Polarity
352.32	32.05	11Z-Eicosenoic acid	1.69E + 10	+
198	20.84	Selenomethionine	6.2E + 07	+
201	18.24	Poppy acid	1.7E + 09	+
159.12	4.87	Betaine	1E + 08	+
758.16	31.69	Theaflavin-3-gallate	4.99E + 09	+
366.96	10.81	Se-Methylselenocysteine	3.78E + 09	+
504	32.86	Quercetin 3,3'-bissulfate	1.22E + 09	+
194.04	4.87	Shoyuflavone A	1.15E + 09	+
720.12	31.69	Norbadione A	7.59E + 08	+
438.72	20.87	Gliadorphin	4.65E + 08	+
312.12	30.79	pinostrobin	4.02E + 09	+
164.04	8.96	Fertaric acid	1.09E + 08	+
339.24	30.93	Plastoquinone 3	2.45E + 08	-
417.12	12.25	Liquiritin	1.3E + 07	-
430.92	10.82	Nitroprusside	2.1E + 09	-
743.04	32.40	Gluconapin	8.3E + 07	-
538.92	12.11	Chymopapain	1.7E + 07	-
179.52	36.15	Glucoputranjivin	1.7E + 07	-
711.62	4.71	Conessine	1.1E + 07	-
889.08	33.10	Baicalin	5E + 06	-
133.08	1.56	3-Butenenitrile	1.5E + 08	-

Table 2. List of Metabolites that are not previously Identified in *T. cordifolia*.

their fragment data. The representative MS/MS spectra and the extracted ion chromatogram of these prominent features are provided in Supplementary Fig. 5 a-d and Table 1. A complete list of unassigned features from positive and negative modes at the MS1 level is shown in Supplementary Tables 5 and 6, respectively. In addition, Supplementary Tables 7 and 8 contain the total unassigned features at the MS/MS level in positive and negative modes, respectively. It's important to note that the significance of reporting these unassigned metabolite features is equivalent to that of mapped metabolites, as they might have functions similar to those of metabolites that are known.

Classification of metabolites based on their cellular localization and chemical class

The metabolites were categorized according to their subcellular location and chemical classifications. As shown in Fig. 2a-c**,** the identified metabolites were classified into superclass, main class, and sub-class. A superclass, such as benzenoids, organic acids, nucleic acids, carbohydrates, alkaloids, etc., main classes, such as phenols, steroids, flavins, ketones, flavonoids etc., and subclass, which includes glycerophosphocholines, glycosphingolipids, benzothiadiazines, ceramide phosphocholines to mention a few. According to the analysis of cellular localization of metabolites, many metabolites were found to be localized in the cytoplasm, followed by the mitochondria, nucleus, membrane, endoplasmic reticulum, golgi apparatus, and peroxisome as represented in Fig. 2d**.**

Metabolite pathway analysis

We used the MetaboAnalyst 5.0 (https://www.metaboanalyst.ca/) online tool to analyze metabolic pathways enriched in *T. cordifolia*. Our results showed the enrichment of several metabolic pathways, including pyrimidine metabolism, sphingolipid metabolism, purine metabolism, cysteine and methionine metabolism, glycerophospholipid metabolism, glutathione metabolism, glycolysis/gluconeogenesis, inositol phosphate metabolism, arachidonic acid metabolism, alanine, aspartate, and glutamate metabolism with $p \leq 0.05$ and are illustrated in Fig. 3a. A detailed list of the metabolite pathways that have been enriched in *T. cordifolia* is provided in Supplementary Table 9.

Protein targets of *T. cordifolia* metabolites

T. cordifolia has been utilized in Ayurvedic formulations to address various health issues for centuries. It brings action in humans through its metabolites. Metabolites regulate multiple biochemical pathways by interacting with various proteins involved in various pathways. Next, we identify human protein targets of *T. cordifolia* metabolites. The metabolites were converted to their corresponding SMILES IDs to identify the protein targets. The BindingDB database (https://www.bindingdb.org/rwd/bind/index.jsp) was used to predict the target proteins of *T. cordifolia*. Using the SMILES ID of the metabolite, BindingDB provided information on protein-metabolite interactions based on metabolite structure and its possible or experimentally proven interaction with a protein. Based on this, We identified a total of 1546 protein interactions, of which 346 were identified with exact structural matches (1.0 score), and 1200 were identified with similarity matches (≥ 0.85 score). The complete list of protein interactions is given in Supplementary Table 10. The identified proteins exhibit diverse functions, including aging, locomotory behavior, learning and memory, cellular response to Aβ, neuronal apoptotic

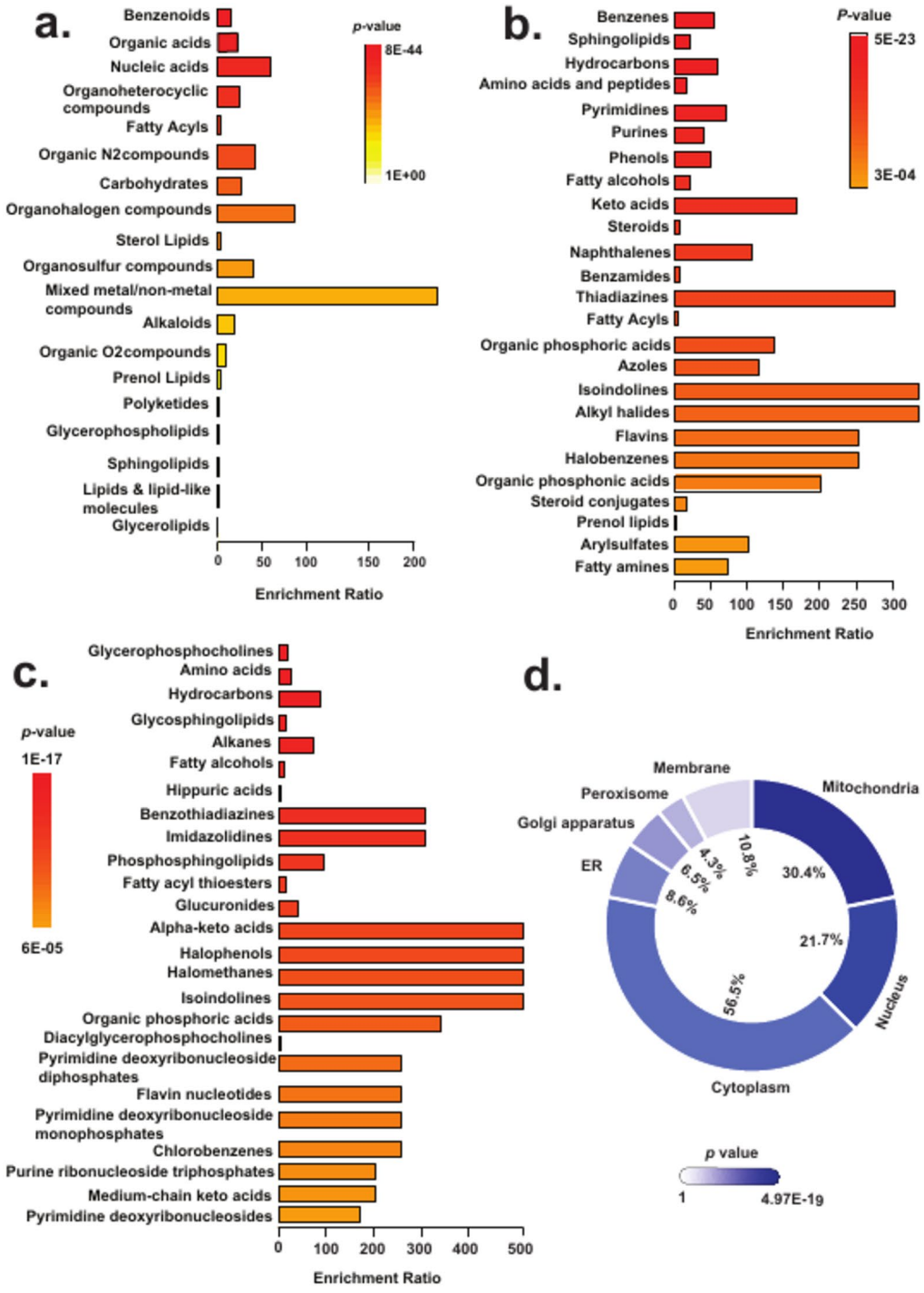

Fig. 2. Metabolite classification based on chemical class. (**a**) Super class, (**b**) Main class, and (**c**) Subclass. (**d**) The doughnut chart represents the classification of metabolites based on cellular location, and shades represent the p-value.

processes, GABAergic and glutamatergic synaptic transmission, neurotransmitter receptor activity, and calcium channel activity, to name a few, as categorized based on their biological processes, subcellular localization, and molecular functions, and depicted in Fig. 3b and Supplementary Table 11.

To predict the human pathways that are induced or altered by *T. cordifolia* metabolites, metabolite–protein joint pathway analysis was carried out. Pathways that are enriched by this analysis include neuroactive ligand-receptor interaction, calcium signaling pathway, serotonergic synapse, cAMP signaling pathway, cholinergic synapse, dopaminergic synapse, apoptosis, PI3K-Akt signaling pathway, neurotrophin signaling pathway, glutamatergic synapse, MAPK signaling pathway, and mTOR signaling pathway to name a few which is represented in Fig. 4a, and a detailed list is provided in Supplementary Table 12.

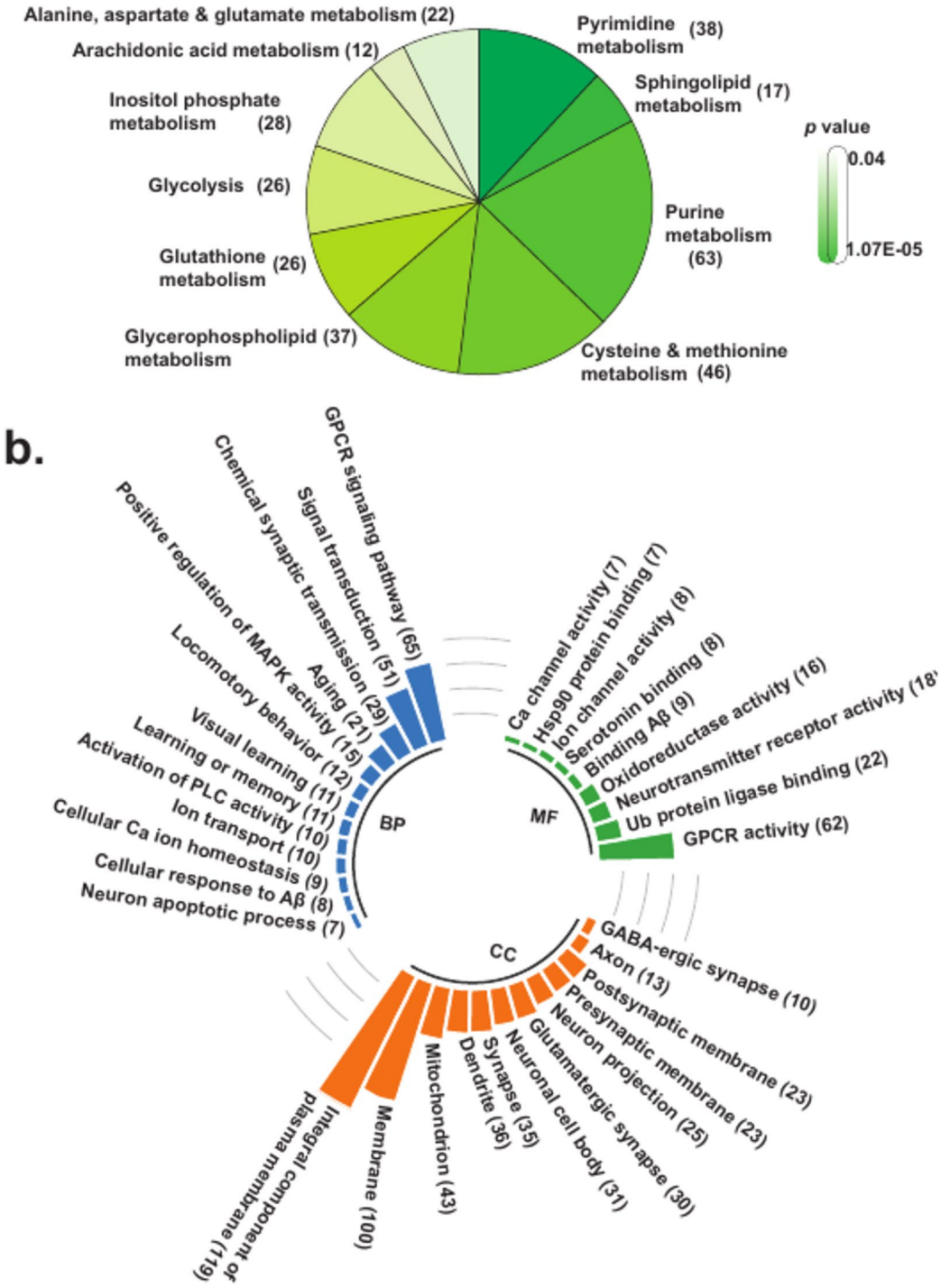

Fig. 3. Analysis of metabolite pathway and proteins interacting with *T. cordifolia* metabolites. (**a**) Pie chart representing the metabolite pathway analysis based on total metabolite coverage, wherein the shades of the slices represent the p-value. (**b**) The Circular bar plot shows human protein classification based on molecular function, biological process, and cellular localization.

The Reactome pathway analysis using the protein targets mapped to the metabolites revealed an abundance of adrenoreceptors, dopamine, serotonin, acetylcholine receptors, neurotransmitter receptors, and postsynaptic signal transmission pathways, which is mentioned in Fig. 4b. Additionally, Fig. 4c displays the enrichment of several important signaling pathways, such as p38MAPK events, MAPK/MAPK2 signaling, RAF activation, Acetylcholine binding, signaling by GPCR, among others. A detailed list is provided in Supplementary Table 13.

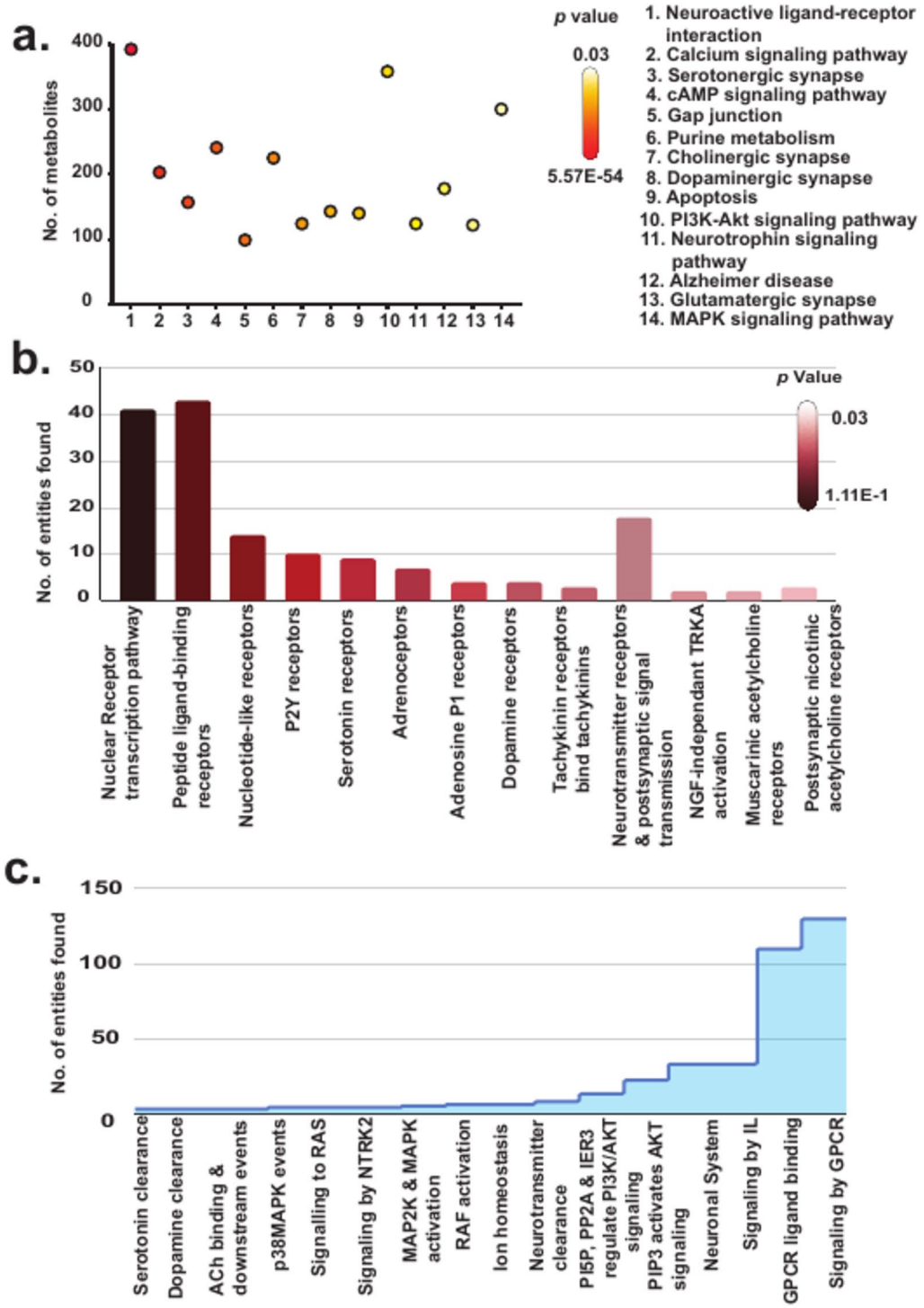

Fig. 4. Analysis of metabolite–protein interaction pathway between the metabolites identified and their target proteins in humans. (**a**) Bubble plot showing the metabolite–protein integrated pathway analysis to predict the pathways in humans that are altered by *T. cordifolia* metabolites, where the X-axis represents the pathway enriched, and the Y-axis represents the number of proteins, (**b**) Coverage of different types of neurotransmitter receptors and the number of proteins identified in each type; X-axis represents the receptor type enriched, and the Y-axis represents the number of proteins, and (**c**) Bar graph showing Reactome pathway analysis of interacting human proteins with metabolites of *T. cordifolia* highlighting several important signaling pathways, the X-axis represents the pathway enriched, and the Y-axis represents the number of proteins entries.

Protein–protein interaction network pharmacology of *T. cordifolia*

We further want to see the protein–protein interaction from identified protein targets of *T. cordifolia* metabolites. This will allow us to understand better how *T. cordifolia* metabolites interact with proteins and bring medicinal effects. We have carried out STRINGdb analysis to construct the protein–protein interaction network to achieve this. The proteins are segregated into four clusters, as shown in Fig. 5, where neurotransmitter receptors are clustered in all four sets of clusters, such as muscarinic acetylcholine receptor M1 (CHRM1), neurotensin receptor type 1 (NTSR1), neuropeptide Y receptor type 2 (NPY2R), dopamine receptor, and neuronal acetylcholine receptor. Glycogen synthase kinase-3 beta (GSK3B), signal transducer and activator of transcription 3 (STAT3), dual specificity mitogen-activated protein kinase kinase 2 (MAP2K2), proto-oncogene tyrosine-protein kinase (SRC), and other significant kinases are also associated in the network. The growth factor receptors such as the

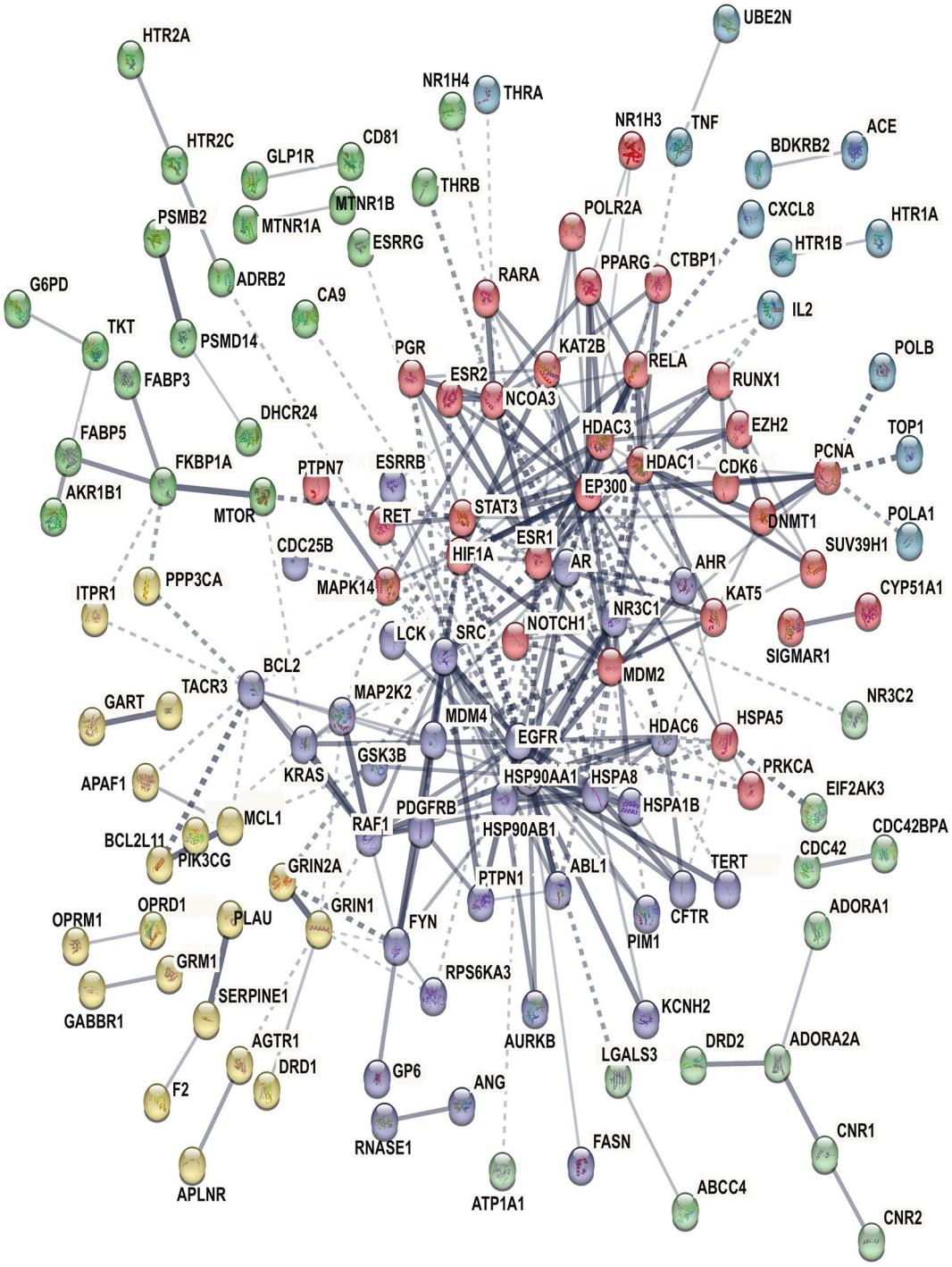

Fig. 5. Network pharmacology of *T. cordifolia*. Protein–protein interacting network of protein targets of *T. cordifolia*.

epidermal growth factor receptor (EGFR), platelet-derived growth factor receptor beta (PDGFRB), and vascular endothelial growth factor receptor 3 (FLT4) are also featured.

Molecular docking leads to the identification of signature metabolites against target proteins involved in Alzheimer's disease

To identify potential inhibitory metabolites in *T. cordifolia* against BACE1 and MAO-B, we conducted molecular docking studies. The results revealed that in BACE1, S-adenosyl-L-methionine demonstrated the highest LibDock score of 124.33 with eight favorable hydrogen bonds, followed by Heptacosan-14-ol (119.104), dUTP (113.38), N-Acetyl-L-arginine (86.74), and (S)-N-Methylcoclaurine (86.29). The reference drug LY2811376, recognized as a BACE1 inhibitor, was also docked at the same active site for comparison. It achieved a lower LibDock score of 72.15 relative to the identified phytocompound. For MAO-B, Palmatine exhibited the highest LibDock score of 114.88 with three favorable hydrogen bonds, followed by n-cis-feruloyl tyramine (111.26), syringin (106.76), sebacic acid (101.82) and choline (52.52). To compare the docking results of the phytocompounds, 8-(3-chlorostyryl) caffeine (CSC), a well-known MAO-B inhibitor, was docked against the defined binding site of the target protein. The findings indicated that 8-(3-chlorostyryl) caffeine (CSC) achieved a LibDock score of 123.87. The high binding scores are attributable to the number and nature of interactions, such as hydrogen bonds, hydrophobic interactions, and π-π stacking, which contribute to the binding stability. For instance, S-adenosyl-L-methionine forms eight favorable hydrogen bonds, enhancing its affinity for BACE1. Similarly, Palmatine's high score is supported by its hydrogen bonding and hydrophobic interactions with MAO-B's active site. These interactions suggest a strong binding potential, which may translate to effective inhibition under physiological conditions. However, their potential side effects need to be explored by conducting in vitro and in vivo experiments. The intermolecular interactions formed between the target proteins and the phytocompound that showed the highest docking score are illustrated in Fig. 6**.** Re-docking of the native ligand against the active site of MAO-B revealed the reliability of the docking protocol. The docking results indicated that the native ligands were exactly bound to the active sites of the target protein. The superimposition of the PDB structure of MAO-B onto the docked complex determined the reliability of the docking protocol with RMSDs of 0 Å.

Validation of neuroprotective activity of *T. cordifolia* in cellular model of Alzheimer's disease

Cytotoxicity of $A\beta_{42}$ peptide and T. cordifolia extract

The treatment dose of $A\beta_{42}$ (0.5 μM) was taken from earlier studies[38]. For *T. cordifolia* extract, IMR-32 cells were treated with different concentrations of *T. cordifolia* triple solvent extract (50 μg/ml to 2000 μg/ml) for 48 h. Our MTT results showed *T. cordifolia* extract to be non-toxic till 500 μg/ml concentration and, at higher concentrations, showed cytotoxicity. Supplementary Fig. 1c. Based on this result, we used 200 μg/ml of *T. cordifolia* triple solvent extract for in vitro studies. Untreated cells were used as the control.

T. cordifolia extract prevents excessive reactive oxygen species (ROS) production and neuronal apoptosis in cellular models of Alzheimer's disease.

In our study, the ROS production in the cells was measured using the dye 2′,7′-DCFDA (2′,7′-dichlorofluorescein diacetate), and live-dead cell staining test was used to determine cell death. Treatment with $A\beta_{42}$ enhanced ROS generation by 7.32-fold ($p \leq 0.001$), which was rescued significantly by *T. cordifolia* co-treatment (2.89-fold $p \leq 0.001$), Fig. 7a&c. The co-treatment of *T. cordifolia* triple solvent extract also reduced cell death caused by $A\beta_{42}$ (7.13-fold, $p \leq 0.001$) by 2.52-fold ($p \leq 0.001$), Fig. 7b&d.

T. cordifolia reversed $A\beta_{42}$-induced alterations of mRNA expression in cellular models of Alzheimer's disease

The qRT-PCR experiments using AChE, MAP2, MAO-B, and ChAT with respect to β-actin genes showed that there was a significant increase in the expression of AChE (2.21-fold, $p \leq 0.01$), MAO-B (1.63-fold, $p \leq 0.05$) genes, and a significant decrease in the expression of ChAT (0.32-fold, $p \leq 0.05$), and MAP 2 (0.69-fold, $p \leq 0.05$) genes expression in the cells treated with $A\beta_{42}$ in Alzheimer's disease condition. Co-treatment with *T. cordifolia* triple solvent extract significantly decreased the AChE (1.26-fold, $p \leq 0.05$) and MAO-B (0.96-fold, $p \leq 0.05$) gene expression and increased the ChAT (1.14-fold, $p \leq 0.01$) and MAP 2 (1.06-fold, $p \leq 0.01$) gene expression compared to $A\beta_{42}$ condition (Fig. 8 a-d). The sequence of primers used in this study is provided in Supplementary Table 14.

T. cordifolia exhibits the potential to reverse abnormal protein alterations associated with Alzheimer's disease pathology

The pathophysiology of Alzheimer's disease (AD) is primarily thought to be caused by aberrant protein accumulation, including phosphorylated tau (p-Tau) deposits that form tangles inside brain cells and β-amyloid peptide (Aβ) deposits that surround brain cells. In this study, we tested the protein accumulation of BACE1, the protein involved in forming Aβ and the p-Tau. β-actin was used as an internal control. Our result showed that in $A\beta_{42}$ treated conditions, these protein expressions were found to be significantly high, BACE 1 (1.58-fold, $p \leq 0.001$) and p-Tau (3.4-fold, $p \leq 0.001$). In contrast, in the co-treatment with *T. cordifolia*, this expression was found to be significantly lower, BACE 1 (0.37-fold, $p \leq 0.001$) and p-Tau (1.35-fold, $p \leq 0.01$). The observed effect may be attributed to the neuroprotective properties of *T. cordifolia* (Fig. 8**. e–g**).

Discussion

Neuroprotection largely refers to improving neuronal health, activity and function to protect them against degenerative or damaging conditions. Most of the current treatments for neurodegenerative diseases such as Alzheimer's and Parkinson's disease are symptomatic, and their effects are ruined as the disease progresses, leading to several side effects and discomfort.

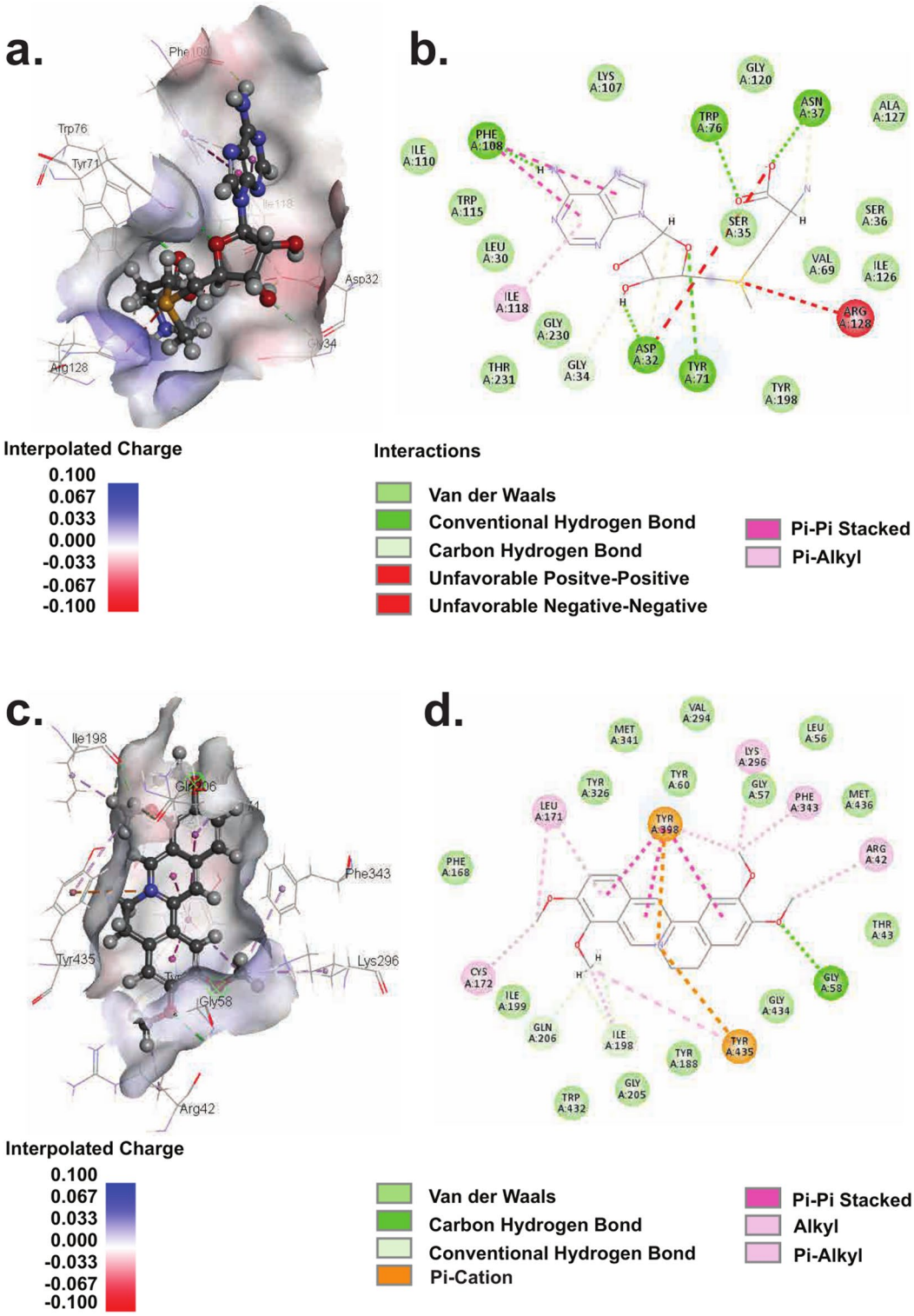

Fig. 6. Phytocompounds interactions with two possible therapeutic target proteins at the molecular level. (**a**) Binding interactions of S-adenosyl-L-methionine against BACE1, (**b**) 2D interaction plot of S-adenosyl-L-methionine against BACE1, (**c**) Binding interactions of Palmatine against MAO-B, (**d**) 2D interaction plot of Palmatine against MAO-B. Binding site residues are labeled, and the phytocompounds are represented in the ball and stick model.

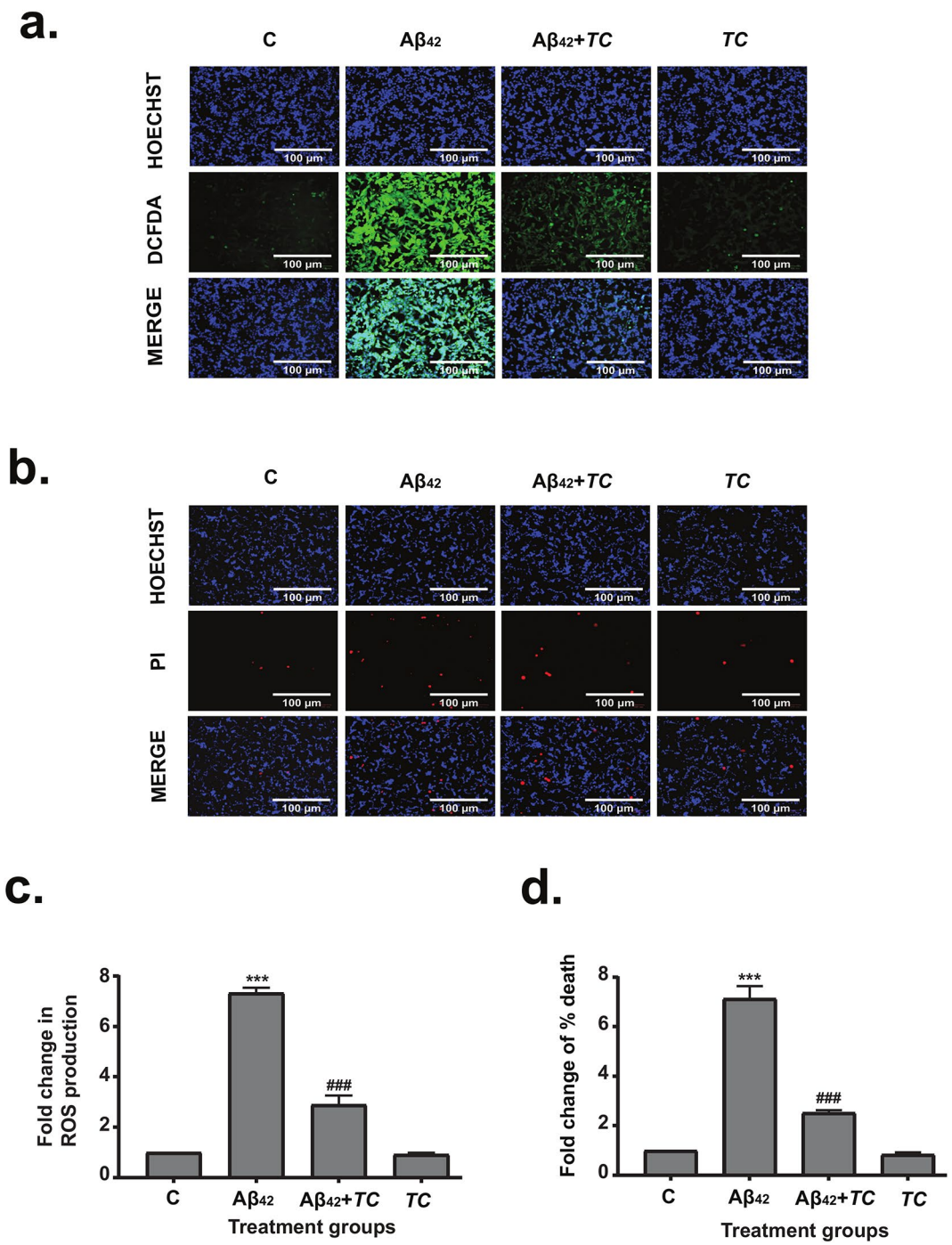

Fig. 7. Detection of oxidative stress and cell apoptosis in IMR-32 cells treated with *T. cordifolia* triple solvent extract. (**a**) Staining of IMR-32 cells using DCFDA: 2',7'–dichlorofluorescin diacetate (green) and counter-stain HOECHST (blue) in the AD model to check the ROS production. (**b**) Staining of IMR-32 cells using propidium iodide (PI) (red) and HOECHST (blue) nuclear counter-stain to check the cell apoptosis in the AD model. (**c**) Graphical representation of ROS production in the IMR-32 cells treated with *T. cordifolia* triple solvent extract in AD model. (**d**) Graphical representation of cell apoptosis with respect to untreated control cells. $A\beta_{42}$ treatment increases cell apoptosis, rescued by *T. cordifolia* triple solvent extract co-treatment. *, significant with respect to control; #, significant with respect to $A\beta_{42}$. ***,### $p \leq 0.001$. Labels: C:-untreated cells, $A\beta_{42}$:- $A\beta_{42}$ treatment, $A\beta_{42}$ + TC:- $A\beta_{42}$ + *T. cordifolia* triple solvent extract co-treatment, TC:- *T. cordifolia* triple solvent extract treatment.

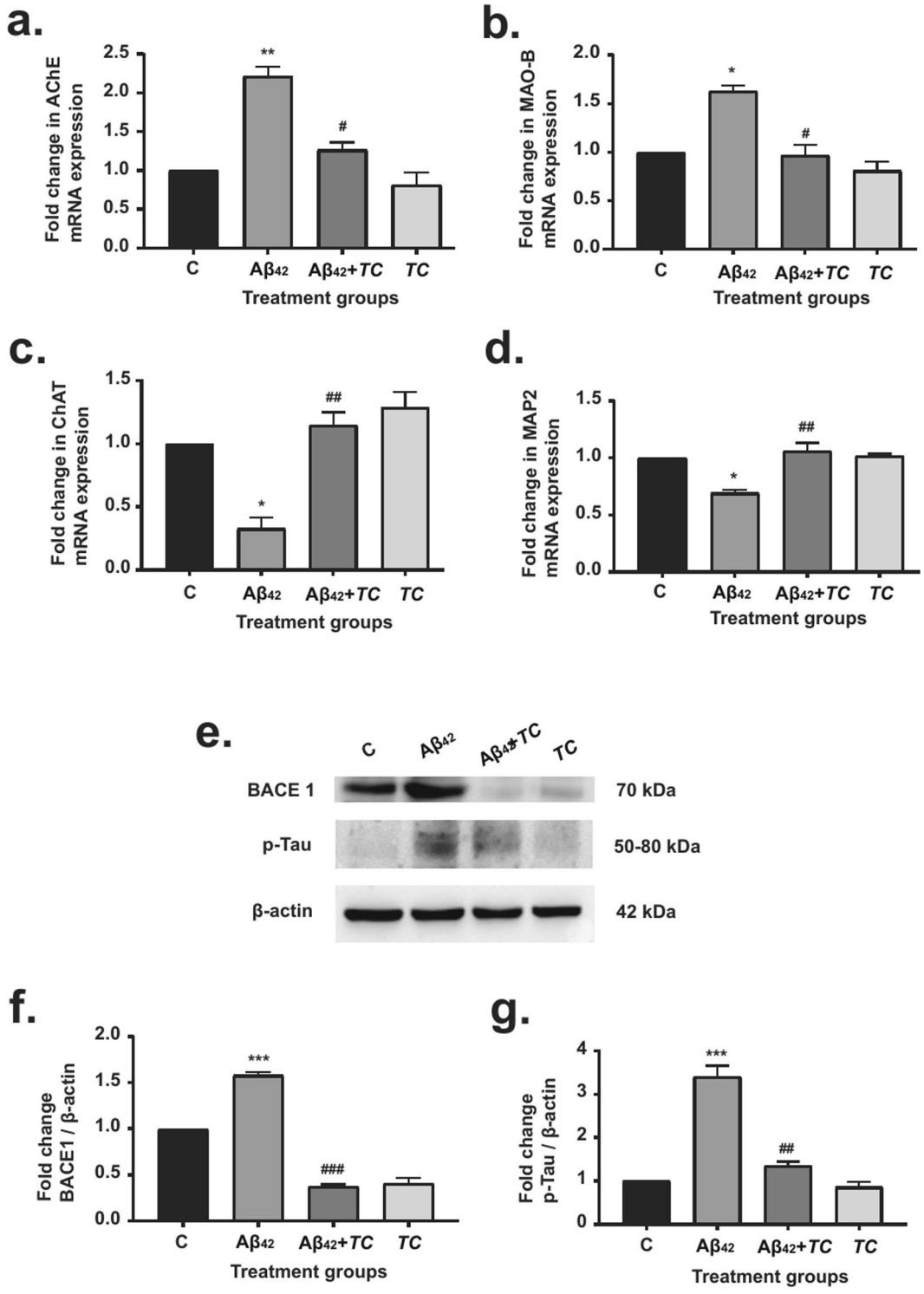

Fig. 8. Effect of *T. cordifolia* on mRNA and protein associated with Alzheimer's disease were analyzed using qRT-PCR and Western blotting, respectively: IMR-32 cells were treated with $A\beta_{42}$ (0.5 µM), $A\beta_{42}$ (0.5 µM) + *T. cordifolia* triple solvent (200 µg/ml), *T. cordifolia* triple solvent extract alone (200 µg/ml), and untreated cells were taken as controls. $A\beta_{42}$ treatment upregulated AChE, MAO-B (mRNA; **a,b**), BACE1, and p-tau (protein; **e–g**) and downregulated ChAT and MAP2 (mRNA; **c,d**) but co-treatment with *T. cordifolia* reversed these effects, suggesting its potential to modulate the disease pathogenesis. (Mean ± SEM, * significant with respect to control; #, significant with respect to $A\beta_{42}$. *,# $p \leq 0.05$, **,## $p \leq 0.01$,***,### $p \leq 0.001$). Labels: C:-untreated cells, $A\beta_{42}$:- $A\beta_{42}$ treatment, $A\beta_{42}$ + TC:- $A\beta_{42}$ + *T. cordifolia* triple solvent extract co-treatment, TC:- *T. cordifolia* triple solvent extract treatment, AChE:- Acetylcholinesterase, ChAT:- Choline Acetyltransferase MAP2:- Microtubule Associated Protein 2, MAO-B:- Monoamine oxidase B, BACE 1: beta-site amyloid precursor protein cleaving enzyme, p-Tau: phosphorylated Tau.

Ayurveda, an ancient system of natural healing that originated in India, offers several herbs and formulations that have been studied for their neuroprotective effects. *T. cordifolia* is a well-known and widely used traditional Indian Ayurvedic medicine known for its beneficial effects[6–19]. It also possesses a variety of secondary plant metabolites, including terpenes, alkaloids, flavonoids, steroids, and glycosides[24,44].

In the current investigation, we carried out untargeted metabolomics and network pharmacology analysis using a mass spectrometry-based metabolomics approach to identify the metabolome-level molecular correlates of *T. cordifolia* and their role in the neuroprotection in Alzheimer's disease.

The present study analyzed secondary metabolites in *T. cordifolia* to see their role in neuroprotection. In Alzheimer's disease (AD), oxidative stress is a significant factor in disturbing the balance between reactive oxygen species (ROS) and the antioxidative defense system. This imbalance increases damage to cellular proteins and lipids[45]. According to the literature, phenolics and flavonoids are the two important secondary metabolites linked to antioxidant activity and associated with a lower risk of several diseases, including Alzheimer's disease[46,47].

Therefore, for our current investigation, we chose to quantify flavonoids and phenolics in *T. cordifolia*. The findings of our study indicate that *T. cordifolia* contains a substantial amount of flavonoids and phenolic compounds known for their antioxidant and potential health-promoting properties. These results suggest that *T. cordifolia* may be a valuable source of natural antioxidants, which may be involved in its neuroprotective properties. Several other natural compounds, such as coumarin-chalcone hybrids, show promise in AD treatment due to their antioxidant activity[48], ability to inhibit Aβ aggregation[49], and selective inhibition of acetylcholinesterase (AChE) activity[50]. Our results showed that the *T. cordifolia* extract also showed neuroprotection in AD, similar to coumarin-chalcone hybrids. The current investigation also reveals that *T. cordifolia* extract effectively alleviates neuronal apoptosis induced by $A\beta_{42}$ in AD to a similar extent, indicating the involvement of another mechanism apart from oxidative stress.

Metabolomics is a powerful tool for analyzing metabolite composition and understanding their roles within a system. Our untargeted metabolomics approach successfully identified several known and metabolites that were not previously reported in *T. cordifolia* extract. We have identified several signature metabolites that are believed to have neuroprotective properties, including syringin, berberine, magnoflorine, choline, S-adenosylmethionine, cryptotanshinone, peonidin, and L-arginine, which were previously reported[6,22,24,51]. Syringin reduces the inflammation associated with cerebral ischemia by mediating the FOXO3a/NF-κB pathway[52] and prevents 6-Hydroxydopamine-induced neurotoxicity[53]; berberine can reduce the activation of caspase-3 and the formation of reactive oxygen species caused by 6-hydroxydopamine in SH-SY5Y cells. Additionally, the Nrf2 expression and neuroprotection-related PI3K/AKT signaling pathway can be activated by berberine[54]. Studies have shown that choline can have neuroprotective effects in animals and humans[55].

S-adenosylmethionine (SAMe) plays a crucial role in various biological processes and serves as a cysteine precursor, methylating agent, biosynthesis and degradation of catecholamines. It is being explored as a therapeutic option for the management of severe neuropsychiatric and neurodegenerative conditions[56]. It improves cognitive function and reduces the accumulation of beta-amyloid plaques in Alzheimer's Disease[57]. Cryptotanshinone (CPT) is a terpenoid reported to have neuroprotective properties against cerebral ischemic stroke[58]. Peonidin is a flavonoid that acts as a neuroprotectant by reducing cell toxicity and inhibiting -synuclein fibrillation, as shown in Parkinson's disease models[59].

Our study also revealed several metabolites identified for the first time in *T. cordifolia*. These metabolites might contribute to its therapeutic potential, such as selenomethionine, the primary form of selenium in foods. Selenium plays an important role in the brain and nervous system, acting as a cofactor for glutathione peroxidase and selenoproteins involved in antioxidant defenses, offering neuroprotective effects through modulation of ROS production and inflammation in various diseases[60]. Betaine restored epigenetic control and alleviated neurological disability in mice by enhancing neuronal respiration and preventing axonal damage[61]. Theaflavin-3-gallate protects biological macromolecules and mitochondrial membrane potential, inhibits aging-related heterochromatin (SAHF)[62], and is also involved in neuroprotection[63]. Se-methyl selenocysteine ameliorates AD-related neuropathology and cognitive deficits in mice by modulating oxidative stress and ERK activation[64]. Pinostrobin reduces chronic stress-induced cognitive impairment, reduces neuronal cell damage and enhances astrocytic function in the hippocampus[65]. Plastoquinone demonstrates superior antioxidant properties and neuroprotective effects in brain ischemia/reperfusion injury in rats[66]. Liquiritin is an excellent antidepressant, and studies also showed that it delays glutamate-injured BV2 cell apoptosis, reduces neuronal cell mortality, and crosses the blood–brain barrier[67]. Baicalin prevents neurodegenerative diseases via antioxidative, anti-excitotoxic, anti-apoptotic, and anti-inflammatory effects and stimulates neurogenesis, showing significant potential in clinical psychiatry by crossing the blood–brain barrier[68].

To investigate the effects of *T. cordifolia* metabolites on the host system, we identified and predicted human proteins that interact with *T. cordifolia* metabolites. This leads to the enrichment of several pathways, such as the calcium signaling pathway, serotonergic, glutamatergic, cholinergic, and dopaminergic synapse, cAMP, PI3K-Akt, MAPK, and mTOR signaling pathway, to name a few. The calcium signaling pathway is critical in various cellular processes, such as muscle contraction, neurotransmitter release, and gene expression, such as calcineurin[69], DISC1, and GAD67[70]. Dysregulation of this pathway has been implicated in various diseases, including cancer and neurological disorders, including Alzheimer's disease[71].

The primary neural routes in the central nervous system are serotonergic, cholinergic, and dopaminergic synapses. The serotonergic synapse uses serotonin neurotransmitter to control mood, cognition, sleep, and appetite. Dysregulation of this pathway has been connected to various psychiatric disorders, including depression and anxiety[72]. The cholinergic synapse uses acetylcholine neurotransmitters to control muscle contraction, attention, learning, and memory; dysregulation of this pathway has been linked to various neurological disorders, including Alzheimer's disease[73]. On the other hand, the dopaminergic synapse uses dopamine neurotransmitters to regulate a variety of physiological processes, including reward, motivation, sleep, dreaming, mood, attention,

working memory, and learning and movement; dysregulation of this pathway has been connected to a variety of neurological and psychiatric disorders, including Parkinson's disease and schizophrenia[74].

cAMP regulates various cellular processes, including metabolism, gene transcription and protein expression, cell growth, and differentiation; dysregulation of this pathway has been implicated in various diseases, including cancer, cardiovascular disease, and neurological disorders[75]. Phosphatidylinositol-3-kinase (PI3K)/Akt and mammalian target of rapamycin (mTOR) signaling pathways are two pathways necessary for numerous aspects of cell growth and survival in both normal and pathological conditions, including neurodegenerative disorders)[76,77]. MAPK pathway also regulates processes such as cell proliferation, cell differentiation, and cell death and is involved in the pathophysiology of AD and PD[78]. Studies have demonstrated that Apelin-13, a prominent neuropeptide with anti-inflammatory properties, significantly ameliorates STZ-induced AD-like phenotypes, including cognitive deficits, cholinergic dysfunction, neuronal and synaptic damage, microglial and astrocytic activation and reduces the expression of inflammatory cytokines (IL-1β and TNF-α) via the BDNF/TrkB pathway[79]. These pathways have been reported to be important in normal brain processes and are known to be dysregulated in neurodegeneration. Since metabolites of *T. cordifolia* regulate the protein involved in these pathways, any aberrant alteration in these pathways in various neurological diseases may be restored by *T. cordifolia*, and hence, it brings neuroprotection.

The protein–protein interaction network helped us understand how the target proteins of metabolites from *T. cordifolia* interact. These interactions network displayed interactions between neurotransmitter receptors like CHRM1, NTSR1, GSK3B, MAP2K2, etc., and kinases like EGFR, PDGFRB, and FLT4 are some of the kinases intertwined in this network. Further research is needed to fully understand the complex interaction and their roles in normal cellular function and disease.

In the present study, some metabolite features remain unassigned as they are not identified in existing datasets or databases. For instance, despite using two plant databases to identify metabolites, some remained unassigned and not fully mapped by these datasets. These unassigned metabolites are as important as the identified ones and require further detailed efforts for characterization.

Our molecular docking results revealed that *T. cordifolia* metabolites exhibited strong binding affinity and favorable interactions with proteins like BACE1 and MAO-B, which are involved in neurodegenerative diseases like Alzheimer's and Parkinson's disease pathology. Specifically, S-adenosyl-L-methionine showed high binding potential with BACE1, while palmatine exhibited strong interactions with MAO-B. Supporting our findings, prior studies have shown that S-adenosylmethionine administration in early Alzheimer's disease reverses hypomethylation and amyloid pathology and restores cognitive capabilities[80]. Palmatine is reported to improve learning and memory in an Alzheimer's disease mouse model, exhibiting blood–brain barrier permeability and restoration of cerebellar and hippocampal proteomes[81], suggesting the identified metabolites and potentially others within the extract hold promise as novel drug candidates. Although this study focused on these two protein targets, the results could be extrapolated to other proteins involved in neurodegeneration, opening doors for discovering new therapeutic targets for neurodegenerative disease.

The in vitro validation of ROS and live-dead assay depicted that *T. cordifolia* could effectively reduce oxidative stress and apoptosis, a major pathological condition seen in AD[82]. Our qRT-PCR results showed that *T. cordifolia* co-treatment significantly downregulates AChE and MAO-B mRNA expression compared to AD conditions. Acetylcholinesterase (AChE) is the enzyme that cleaves acetylcholine neurotransmitters, and the present treatment of Alzheimer's disease is based on the use of acetylcholinesterase (AChE) inhibitors[83]. On the other hand, MAO-B enzymatic activity generates hydrogen peroxide, resulting in the production of reactive oxygen species (ROS)[84]. Expressions of AChE and MAO-B are found to be high in AD conditions[85,86]. We also observed an increase in the expression of Choline acetyltransferase (ChAT) and Microtubule-associated protein 2 (MAP2) upon co-treatment with *T. cordifolia* compared to AD condition. ChAT is responsible for the synthesis of ACh from acetyl-CoA and choline. MAP2 stabilizes the microtubules in the dendrites, regulates synaptic plasticity and can serve as a marker or effecter of neuronal death[87]. These two proteins' expressions are found to be decreased in AD[73,88]. The other key proteins involved in Alzheimer's disease (AD) pathology are β-secretase BACE1 (β-site APP cleaving enzyme) and hyperphosphorylated tau protein. BACE1 cleaves the transmembrane amyloid precursor protein (APP) together with γ-secretase to generate amyloid β (Aβ) peptide, which in AD conditions is seen to be increasingly large and regionally deposited as brain aggregates[89,90]. Aβ influences the aggregation of tau protein, and these protein abnormalities are thought to contribute to the cognitive decline seen in AD patients[91]. Our study indicated that co-treatment with *T. cordifolia* significantly reduced the BACE1 and p-Tau protein levels in western blotting analysis. These findings collectively suggest the potential of *T. cordifolia* as a neuroprotective agent. By influencing the expression of these proteins and mRNA, *T. cordifolia* may offer neuroprotection against Alzheimer's disease pathology.

Other than these proteins, multiple kinases, including MST1/2, PKCα, GSK3B, CDK5, p38 MAPK, JNK, and ERK1/2, have been implicated in Alzheimer's Disease (AD) pathogenesis. Studies have shown that their dysregulation contributes to various aspects of the disease, including Aβ accumulation, synaptic dysfunction, tau phosphorylation, neuroinflammation, and neuronal death. For instance, overexpression of MST1/2 and PKCα leads to cognitive decline, synaptic impairment, and neuronal apoptosis[76,92]. Additionally, hyperactivation of GSK3B and CDK5, as well as dysregulation of p38 MAPK, JNK, and ERK1/2, have all been linked to key pathological features of AD[93–97].

The pharmacological significance of *T. cordifolia* is attributed to its phytoconstituents, which include alkaloids, glycosides, diterpene lactones, steroids, phenolics, sesquiterpenoids, aliphatic compounds, and polysaccharides[98]. These compounds have been reported to exhibit diverse bioactivities in both in vitro and in vivo preclinical model systems. The alkaloids, terpenoids, sitosterols, flavonoids, and phenolic acids found in *T. cordifolia* activate Nrf2, leading to the overexpression of various antioxidant enzymes and helping induce an adaptive response to oxidative stress. *T. cordifolia* also reduces NF-κB signaling by inhibiting PI3K/Akt, activating AMPK

and sirtuins, and downregulating PI3K/Akt[23]. Another study reports that G1-4A, a polysaccharide isolated from *T. cordifolia* stems, modulated the defensive host immune response in the RAW 264.7 macrophage cell line[99] and also reduced pro-inflammatory cytokine levels (TNF-α, IL-1β, IL-6, and IFN-γ) and NO release in mice[100]. Methanolic fraction of *T. cordifolia* exhibited potent acetylcholinesterase (AChE) inhibition, likely attributed to the synergistic effects of its isoquinoline alkaloids. The presence of palmatine and berberine both show superior AChE inhibitory activity compared to gallic acid and the standard drug galantamine hydrobromide[21]. Based on these findings, it is evident that *T. cordifolia* has the potential for various clinical applications that may be explored in detail by conducting clinical trials.

The current study has provided valuable insights into the complex biochemical pathways and metabolic processes involved in the plant's therapeutic effects. It has also helped to identify potential bioactive compounds that could be developed as novel therapeutic agents for various diseases, including neurodegenerative diseases, particularly Alzheimer's disease.

However, further in vitro and in vivo validation is needed to fully understand the metabolic pathways and mechanisms underlying the therapeutic effects of *T. cordifolia*. In particular, more research is required to determine the pharmacokinetics and pharmacodynamics of the bioactive compounds identified in *T. cordifolia*. This will help to determine the optimal dosage and delivery methods for these compounds to maximize their therapeutic effects.

The integration of network pharmacology with metabolomics focuses on understanding drug mechanisms through biomolecular networks, leading to advancements in drug discovery and development[101,102]. Furthermore, the inclusion of docking studies enhanced this understanding by identifying potential interactions of metabolites within the host system, aiding in the drug development process. The untargeted metabolomics profiling provided insights into the several therapeutic effects of the constituents of *T. cordifolia*. Further, we used network pharmacology to find out the probable mechanisms of the plant constituents that could act to counter the pathogenesis of Alzheimer's disease. While this untargeted metabolomic study demonstrates the neuroprotective effects of *T. cordifolia* and validates them in vitro, further in vivo validation is crucial for clinical translation. This study serves as a stepping stone for future research in this area.

In conclusion, metabolomics studies on *T. cordifolia* have provided valuable insights into the plant's medicinal properties and have identified potential bioactive compounds that could be developed as novel therapeutic agents for various diseases. Our work represents only the beginning, highlighting the need for enhanced metabolite databases to reduce the number of unidentified metabolites. Further exploration and improvements in these databases will help better identify and understand these metabolites. The active metabolites of *T. cordifolia* can be quantified using targeted mass spectrometry-based methods such as Multiple Reaction Monitoring (MRM) or Parallel Reaction Monitoring (PRM). Additional studies are needed to fully understand the mechanisms underlying the therapeutic effects of *T. cordifolia* and to determine the safety and efficacy of the plant and its bioactive compounds in clinical settings.

Data availability

All the data is available in the manuscript and supplementary information. The mass spectrometry raw data have been submitted to MassIVE—Mass Spectrometry Interactive Virtual Environment (https://massive.ucsd.edu), with the study identifier MSV000096283.

Received: 5 November 2024; Accepted: 3 March 2025
Published online: 08 March 2025

References

1. Huang, Z. et al. An ayurgenomics approach: Prakriti-based drug discovery and development for personalized care. *Front. Pharmacol.* **13**, 866827 (2022).
2. Sharma, B. & Yadav, D. K. Metabolomics and network pharmacology in the exploration of the multi-targeted therapeutic approach of traditional medicinal plants. *Plants (Basel)* **11**, 3243 (2022).
3. Hopkins, A. L. Network pharmacology: The next paradigm in drug discovery. *Nat. Chem. Biol.* **4**, 682–690 (2008).
4. Nakabayashi, R. & Saito, K. Metabolomics for unknown plant metabolites. *Anal. Bioanal. Chem.* **405**, 5005–5011 (2013).
5. Kulkarni, R., Girish, K. J. & Kumar, A. Nootropic herbs (Medhya Rasayana) in ayurveda: An update. *Pharmacogn. Rev.* **6**, 147–153 (2012).
6. Upadhyay, A. K., Kumar, K., Kumar, A. & Mishra, H. S. Tinospora cordifolia (willd.) hook. f. and thoms. (guduchi) - validation of the ayurvedic pharmacology through experimental and clinical studies. *Int. J. Ayurveda Res.* **1**, 112–121 (2010).
7. Sharma, U. et al. Immunomodulatory active compounds from Tinospora cordifolia. *J. Ethnopharmacol.* **141**, 918–926 (2012).
8. Wesley, J., Christina, A., Chidambaranathan, N., Livingston, R. & Ravikumar, K. Effect of alcoholic extract of Tinospora cordifolia on acute and subacute inflammation. *Pharmacologyonline* **3**, 683–687 (2008).
9. Prince, P. S., Kamalakkannan, N. & Menon, V. P. Restoration of antioxidants by ethanolic Tinospora cordifolia in alloxan-induced diabetic wistar rats. *Acta Pol. Pharm.* **61**, 283–287 (2004).
10. Nagarkatti, D. S., Rege, N. N., Desai, N. K. & Dahanukar, S. A. Modulation of kupffer cell activity by Tinospora cordifolia in liver damage. *J. Postgrad. Med.* **40**, 65–67 (1994).
11. Stanely, P., Prince, M. & Menon, V. P. Hypoglycaemic and other related actions of Tinospora cordifolia roots in alloxan-induced diabetic rats. *J. Ethnopharmacol.* **70**, 9–15 (2000).
12. Bonvicini, F., Mandrone, M., Antognoni, F., Poli, F. & Gentilomi, G. A. Ethanolic extracts of Tinospora cordifolia and alstonia scholaris show antimicrobial activity towards clinical isolates of methicillin-resistant and carbapenemase-producing bacteria. *Nat. Prod. Res.* **28**, 1438–1445 (2014).
13. Stanely Mainzen Prince, P., Menon, V. P. & Gunasekaran, G. Hypolipidaemic action of Tinospora cordifolia roots in alloxan diabetic rats. *J. Ethnopharmacol.* **64**, 53–57 (1999).
14. Hussain, L., Akash, M. S., Ain, N. U., Rehman, K. & Ibrahim, M. The analgesic, anti-inflammatory and anti-pyretic activities of Tinospora cordifolia. *Adv. Clin. Exp. Med.* **24**, 957–964 (2015).
15. Rao, P. R., Kumar, V. K., Viswanath, R. K. & Subbaraju, G. V. Cardioprotective activity of alcoholic extract of Tinospora cordifolia in ischemia-reperfusion induced myocardial infarction in rats. *Biol. Pharm. Bull.* **28**, 2319–2322 (2005).

16. Birla, H. et al. Unraveling the neuroprotective effect of Tinospora cordifolia in a parkinsonian mouse model through the proteomics approach. *ACS Chem. Neurosci.* **12**, 4319–4335 (2021).
17. Kapur, P., Jarry, H., Wuttke, W., Pereira, B. M. & Seidlova-Wuttke, D. Evaluation of the antiosteoporotic potential of Tinospora cordifolia in female rats. *Maturitas* **59**, 329–338 (2008).
18. Jagetia, G. C., Nayak, V. & Vidyasagar, M. S. Evaluation of the antineoplastic activity of guduchi (Tinospora cordifolia) in cultured HeLa cells. *Cancer Lett.* **127**, 71–82 (1998).
19. Jyothi, C., Shashikala, G., Vidya, H. & Shashikala, G. Evaluation of effect of alcoholic extract of Tinospora cordifolia on learning and memory in alprazolam induced amnesia in albino mice. *Int. J. Basic Clin. Pharmacol.* **5**, 2159–2164 (2016).
20. Bhalodi, K. & Kothari, C. S. Tinospora cordifolia: A new perspective on alzheimer's disease and green nanotechnology. *Nat. Prod. J.* **13**, 26–39 (2023).
21. Vinutha, B. et al. Screening of selected Indian medicinal plants for acetylcholinesterase inhibitory activity. *J. Ethnopharmacol.* **109**, 359–363 (2007).
22. Sharma, A. & Kaur, G. Tinospora cordifolia as a potential neuroregenerative candidate against glutamate induced excitotoxicity: an in vitro perspective. *BMC Complement Altern. Med.* **18**, 268 (2018).
23. Arunachalam, K., Yang, X. & San, T. T. Tinospora cordifolia (willd) Miers: Protection mechanisms and strategies against oxidative stress-related diseases. *J. Ethnopharmacol.* https://doi.org/10.1016/j.jep.2021.114540 (2022).
24. Saeed, M. et al. Using guduchi (Tinospora cordifolia) as an eco-friendly feed supplement in human and poultry nutrition. *Poult. Sci.* **99**, 801–811 (2020).
25. da Silva, L. A., Pezzini, B. R. & Soares, L. Spectrophotometric determination of the total flavonoid content in Ocimum basilicum L. (lamiaceae) leaves. *Pharmacogn. Mag.* **11**, 96–101 (2015).
26. Bray, H. G. & Thorpe, W. V. Analysis of phenolic compounds of interest in metabolism. *Methods Biochem. Anal.* **1**, 27–52 (1954).
27. Karthikkeyan, G. et al. Plant omics: Metabolomics and network pharmacology of liquorice. *Indian Ayurvedic Med. Yashtimadhu. OMICS* **24**, 743–755 (2020).
28. Song, Y., Yang, X., Jiang, Y. & Tu, P. Characterization of the metabolism of sibiricaxanthone F and its aglycone in vitro by high performance liquid chromatography coupled with Q-trap mass spectrometry. *J. Pharm. Biomed. Anal.* **70**, 700–707 (2012).
29. Li, C. et al. Precursor ion scan enhanced rapid identification of the chemical constituents of danhong injection by liquid chromatography-tandem mass spectrometry: An integrated strategy. *J. Chromatogr. A* **1602**, 378–385 (2019).
30. Chambers, M. C. et al. A cross-platform toolkit for mass spectrometry and proteomics. *Nat. Biotechnol.* **30**, 918–920 (2012).
31. Pluskal, T., Castillo, S., Villar-Briones, A. & Oresic, M. MZmine 2: Modular framework for processing, visualizing, and analyzing mass spectrometry-based molecular profile data. *BMC Bioinform.* **11**, 395 (2010).
32. Kanehisa, M. & Goto, S. KEGG: Kyoto encyclopedia of genes and genomes. *Nucleic Acids Res.* **28**, 27–30 (2000).
33. Kanehisa, M., Furumichi, M., Sato, Y., Matsuura, Y. & Ishiguro-Watanabe, M. KEGG: Biological systems database as a model of the real world. *Nucleic Acids Res.* **53**, D672–D677 (2025).
34. Behera, S. K. et al. MS2Compound: A user-friendly compound identification tool for LC-MS/MS-based metabolomics data. *OMICS* **25**, 389–399 (2021).
35. Pang, Z. et al. MetaboAnalyst 5.0: Narrowing the gap between raw spectra and functional insights. *Nucleic Acids Res.* **49**, W388–W396 (2021).
36. Lopez-Ibanez, J., Pazos, F. & Chagoyen, M. MBROLE 2.0-functional enrichment of chemical compounds. *Nucleic Acids Res.* **44**, W201-204 (2016).
37. Gilson, M. K. et al. BindingDB in 2015: A public database for medicinal chemistry, computational chemistry and systems pharmacology. *Nucleic Acids Res.* **44**, D1045-1053 (2016).
38. Parate, S. S. et al. Comparative metabolomics and network pharmacology analysis reveal shared neuroprotective mechanisms of Bacopa monnieri (L.) Wettst and Centella asiatica (L.) Urb. *Mol. Neurobiol.* **5**, 1–23 (2024).
39. Karthikkeyan, G. et al. Data on dose-dependent cytotoxicity of rotenone and neuroprotection conferred by Yashtimadhu (Glycyrrhiza glabra L.) in an in vitro Parkinson's disease model. *Data Brief* **39**, 107535 (2021).
40. Karthikkeyan, G., Pervaje, R., Pervaje, S. K., Prasad, T. S. K. & Modi, P. K. Prevention of MEK-ERK-1/2 hyper-activation underlines the neuroprotective effect of Glycyrrhiza glabra L. (Yashtimadhu) against rotenone-induced cellular and molecular aberrations. *J. Ethnopharmacol.* https://doi.org/10.1016/j.jep.2021.114025 (2021).
41. Modi, P. K. & Kanungo, M. S. Age-dependent expression of S100beta in the brain of mice. *Cell. Mol. Neurobiol.* **30**, 709–716 (2010).
42. Yan, R. & Vassar, R. Targeting the beta secretase BACE1 for Alzheimer's disease therapy. *Lancet Neurol.* **13**, 319–329 (2014).
43. Behl, T. et al. Role of monoamine oxidase activity in Alzheimer's disease: An insight into the therapeutic potential of inhibitors. *Molecules* https://doi.org/10.3390/molecules26123724 (2021).
44. Singh, D. & Chaudhuri, P. K. Chemistry and pharmacology of Tinospora cordifolia. *Nat. Prod. Commun.* **12**, 299–308 (2017).
45. Sharma, C. & Kim, S. R. Linking oxidative stress and proteinopathy in Alzheimer's disease. *Antioxidants (Basel)* https://doi.org/10.3390/antiox10081231 (2021).
46. Hole, K. L. & Williams, R. J. Flavonoids as an intervention for Alzheimer's disease: Progress and hurdles towards defining a mechanism of action. *Brain Plast.* **6**, 167–192 (2021).
47. Bukhari, S. N. A. Dietary polyphenols as therapeutic intervention for Alzheimer's disease: A mechanistic insight. *Antioxidants (Basel)* https://doi.org/10.3390/antiox11030554 (2022).
48. Bensalah, D., Amri, N., Mukhrish, Y. E., Koko, W. S. & Hamdi, N. Synthesis and pharmacological properties of coumarin-chalcones. *MethodsX* **11**, 102488 (2023).
49. Lee, S. Y. et al. Novel synthetic chalcone-coumarin hybrid for abeta aggregation reduction, antioxidation, and neuroprotection. *CNS Neurosci. Ther.* **24**, 1286–1298 (2018).
50. Kang, L. et al. Structure-activity relationship investigation of coumarin-chalcone hybrids with diverse side-chains as acetylcholinesterase and butyrylcholinesterase inhibitors. *Mol. Divers.* **22**, 893–906 (2018).
51. Shirolkar, A., Sharma, B., Lata, S. & Dabur, R. Guduchi sawras (Tinospora cordifolia): An Ayurvedic drug treatment modulates the impaired lipid metabolism in alcoholics through dopaminergic neurotransmission and anti-oxidant defense system. *Biomed. Pharmacother.* **83**, 1265–1277 (2016).
52. Liu, Y., Zhu, X., Tong, X. & Tan, Z. Syringin protects against cerebral ischemia/reperfusion injury via inhibiting neuroinflammation and TLR4 signaling. *Perfusion* **37**, 562–569 (2022).
53. Fu, R. H., Hong, S. Y. & Chen, H. J. Syringin prevents 6-hydroxydopamine neurotoxicity by mediating the MiR-34a/SIRT1/beclin-1 pathway and activating autophagy in SH-SY5Y cells and the Caenorhabditis elegans model. *Cells* https://doi.org/10.3390/cells12182310 (2023).
54. Bae, J. et al. Berberine protects 6-hydroxydopamine-induced human dopaminergic neuronal cell death through the induction of heme oxygenase-1. *Mol. Cells* **35**, 151–157 (2013).
55. Blusztajn, J. K., Slack, B. E. & Mellott, T. J. Neuroprotective actions of dietary choline. *Nutrients* https://doi.org/10.3390/nu9080815 (2017).
56. Gao, J. et al. S-Adenosyl methionine and transmethylation pathways in neuropsychiatric diseases throughout life. *Neurotherapeutics* **15**, 156–175 (2018).
57. Fuso, A. et al. S-adenosylmethionine reduces the progress of the Alzheimer-like features induced by B-vitamin deficiency in mice. *Neurobiol. Aging* **33**, 1482-e1 (2012).

58. Xu, D., Gui, C., Zhao, H. & Liu, F. Cryptotanshinone protects hippocampal neurons against oxygen-glucose deprivation-induced injury through the activation of Nrf2/HO-1 signaling pathway. *Food Sci. Technol.* **42**, e46521 (2021).
59. Verma, G. & Bhat, R. The anthocyanidin peonidin interferes with an early step in the fibrillation pathway of alpha-synuclein and modulates it toward amorphous aggregates. *ACS Chem. Neurosci.* https://doi.org/10.1021/acschemneuro.2c00726 (2023).
60. Song, G. et al. Selenomethionine ameliorates cognitive decline, reduces tau hyperphosphorylation, and reverses synaptic deficit in the triple transgenic mouse model of Alzheimer's disease. *J. Alzheimers Dis.* **41**, 85–99 (2014).
61. Singhal, N. K. et al. Betaine restores epigenetic control and supports neuronal mitochondria in the cuprizone mouse model of multiple sclerosis. *Epigenetics* **15**, 871–886 (2020).
62. Zheng, X. et al. Anti-damage effect of theaflavin-3'-gallate from black tea on UVB-irradiated HaCaT cells by photoprotection and maintaining cell homeostasis. *J. Photochem. Photobiol. B* **224**, 112304 (2021).
63. Zhang, J. et al. Neuroprotective effects of theaflavins against oxidative stress-induced apoptosis in PC12 cells. *Neurochem. Res.* **41**, 3364–3372 (2016).
64. Xie, Y. et al. Se-Methylselenocysteine ameliorates neuropathology and cognitive deficits by attenuating oxidative stress and metal dyshomeostasis in Alzheimer model mice. *Mol. Nutr. Food Res.* **62**, e1800107 (2018).
65. Thongrong, S., Surapinit, S., Promsrisuk, T., Jittiwat, J. & Kongsui, R. Pinostrobin alleviates chronic restraint stress-induced cognitive impairment by modulating oxidative stress and the function of astrocytes in the hippocampus of rats. *Biomed. Rep.* **18**, 20 (2023).
66. Silachev, D. N. et al. Neuroprotective effects of mitochondria-targeted plastoquinone and thymoquinone in a rat model of brain ischemia/reperfusion injury. *Molecules* **20**, 14487–14503 (2015).
67. Qin, J. et al. Pharmacological activities and pharmacokinetics of liquiritin: A review. *J. Ethnopharmacol.* **293**, 115257 (2022).
68. Sowndhararajan, K., Deepa, P., Kim, M., Park, S. J. & Kim, S. Neuroprotective and cognitive enhancement potentials of baicalin: A review. *Brain Sci.* **8**, 104 (2018).
69. Foster, T. C., Sharrow, K. M., Masse, J. R., Norris, C. M. & Kumar, A. Calcineurin links Ca2+ dysregulation with brain aging. *J. Neurosci.* **21**, 4066–4073 (2001).
70. Berridge, M. J. Dysregulation of neural calcium signaling in Alzheimer disease, bipolar disorder and schizophrenia. *Prion* **7**, 2–13 (2013).
71. Berridge, M. J. Calcium signalling remodelling and disease. *Biochem. Soc. Trans.* **40**, 297–309 (2012).
72. Jenkins, T. A., Nguyen, J. C., Polglaze, K. E. & Bertrand, P. P. Influence of tryptophan and serotonin on mood and cognition with a possible role of the gut-brain axis. *Nutrients* https://doi.org/10.3390/nu8010056 (2016).
73. Ferreira-Vieira, T. H., Guimaraes, I. M., Silva, F. R. & Ribeiro, F. M. Alzheimer's disease: Targeting the cholinergic system. *Curr. Neuropharmacol.* **14**, 101–115 (2016).
74. Juarez Olguin, H., Calderon Guzman, D., Hernandez Garcia, E. & Barragan, M. G. The role of dopamine and its dysfunction as a consequence of oxidative stress. *Oxid. Med. Cell. Longev.* **2016**, 9730467 (2016).
75. Yan, K., Gao, L. N., Cui, Y. L., Zhang, Y. & Zhou, X. The cyclic AMP signaling pathway: Exploring targets for successful drug discovery (Review). *Mol. Med. Rep.* **13**, 3715–3723 (2016).
76. Wong, M. Mammalian target of rapamycin (mTOR) pathways in neurological diseases. *Biomed. J.* **36**, 40–50 (2013).
77. Long, H. Z. et al. PI3K/AKT signal pathway: A target of natural products in the prevention and treatment of Alzheimer's disease and parkinson's disease. *Front. Pharmacol.* **12**, 648636 (2021).
78. Morrison, D. K. MAP kinase pathways. *Cold Spring Harb. Perspect. Biol.* https://doi.org/10.1101/cshperspect.a011254 (2012).
79. Luo, H. et al. Apelin-13 suppresses neuroinflammation against cognitive deficit in a streptozotocin-induced rat model of Alzheimer's disease through activation of BDNF-TrkB signaling pathway. *Front. Pharmacol.* **10**, 395 (2019).
80. Do Carmo, S. et al. Rescue of early bace-1 and global DNA demethylation by S-adenosylmethionine reduces amyloid pathology and improves cognition in an Alzheimer's model. *Sci. Rep.* **6**, 34051 (2016).
81. Kiris, I. et al. Proteomic alterations in the cerebellum and hippocampus in an Alzheimer's disease mouse model: Alleviating effect of palmatine. *Biomed. Pharmacother.* **158**, 114111 (2023).
82. Gella, A. & Durany, N. Oxidative stress in Alzheimer disease. *Cell Adh. Migr.* **3**, 88–93 (2009).
83. Rees, T. M. & Brimijoin, S. The role of acetylcholinesterase in the pathogenesis of Alzheimer's disease. *Drugs Today (Barc)* **39**, 75–83 (2003).
84. Chun, H. et al. Severe reactive astrocytes precipitate pathological hallmarks of Alzheimer's disease via H(2)O(2)(-) production. *Nat. Neurosci.* **23**, 1555–1566 (2020).
85. Jaisa-Aad, M., Munoz-Castro, C., Healey, M. A., Hyman, B. T. & Serrano-Pozo, A. Characterization of monoamine oxidase-B (MAO-B) as a biomarker of reactive astrogliosis in Alzheimer's disease and related dementias. *Acta Neuropathol.* **147**, 66 (2024).
86. Campanari, M. L. et al. Increased expression of readthrough acetylcholinesterase variants in the brains of Alzheimer's disease patients. *J. Alzheimers Dis.* **53**, 831–841 (2016).
87. DeGiosio, R. A. et al. More than a marker: Potential pathogenic functions of MAP2. *Front. Mol. Neurosci.* **15**, 974890 (2022).
88. Zhang, J. & Dong, X. P. Dysfunction of microtubule-associated proteins of MAP2/tau family in Prion disease. *Prion* **6**, 334–338 (2012).
89. Shah, H. et al. The β-Secretase Enzyme BACE1: A biochemical enigma for Alzheimer's disease. *CNS Neurol. Disord. Drug Targets* **19**, 184–194 (2020).
90. Medeiros, R., Baglietto-Vargas, D. & LaFerla, F. M. The role of tau in Alzheimer's disease and related disorders. *CNS Neurosci. Ther.* **17**, 514–524 (2011).
91. Zhang, H. et al. Interaction between abeta and tau in the pathogenesis of Alzheimer's disease. *Int. J. Biol. Sci.* **17**, 2181–2192 (2021).
92. Lorden, G. et al. Enhanced activity of Alzheimer disease-associated variant of protein kinase calpha drives cognitive decline in a mouse model. *Nat. Commun.* **13**, 7200 (2022).
93. Lauretti, E., Dincer, O. & Pratico, D. Glycogen synthase kinase-3 signaling in Alzheimer's disease. *Biochim. Biophys. Acta Mol. Cell Res.* **1867**, 118664 (2020).
94. Liu, S. L. et al. The role of Cdk5 in Alzheimer's disease. *Mol. Neurobiol.* **53**, 4328–4342 (2016).
95. Munoz, L. & Ammit, A. J. Targeting p38 MAPK pathway for the treatment of Alzheimer's disease. *Neuropharmacology* **58**, 561–568 (2010).
96. Solas, M. et al. JNK activation in Alzheimer's disease is driven by amyloid beta and is associated with tau pathology. *ACS Chem. Neurosci.* **14**, 1524–1534 (2023).
97. Khezri, M. R., Yousefi, K., Esmaeili, A. & Ghasemnejad-Berenji, M. The role of ERK1/2 pathway in the pathophysiology of Alzheimer's disease: An overview and update on new developments. *Cell Mol. Neurobiol.* **43**, 177–191 (2023).
98. Sharma, A., Bajaj, P., Bhandari, A. & Kaur, G. From ayurvedic folk medicine to preclinical neurotherapeutic role of a miraculous herb, Tinospora cordifolia. *Neurochem. Int.* **141**, 104891 (2020).
99. Raghu, R. et al. Molecular events in the activation of B cells and macrophages by a non-microbial TLR4 agonist, G1–4A from Tinospora cordifolia. *Immunol. Lett.* **123**, 60–71 (2009).
100. Desai, V. R., Ramkrishnan, R., Chintalwar, G. J. & Sainis, K. B. G1–4A, an immunomodulatory polysaccharide from Tinospora cordifolia, modulates macrophage responses and protects mice against lipopolysaccharide induced endotoxic shock. *Int. Immunopharmacol.* **7**, 1375–1386 (2007).
101. Lai, X. et al. Editorial: Network pharmacology and traditional medicine. *Front. Pharmacol.* **11**, 1194 (2020).

102. Wang, Z. Y., Wang, X., Zhang, D. Y., Hu, Y. J. & Li, S. Traditional Chinese medicine network pharmacology: development in new era under guidance of network pharmacology evaluation method guidance. *Zhongguo Zhong Yao Za Zhi* **47**, 7–17 (2022).

Acknowledgements
The authors acknowledge the support of the Department of Biotechnology, Government of India, to the Yenepoya (Deemed to be University) through the project on "Skill Development in Mass Spectrometry based metabolomics technology BIC" (BT/PR40202/BTIS/137/53/2023). We also thank Karnataka Biotechnology and Information Technology Services (KBITS), the Government of Karnataka, for the infrastructure support of the Center for Systems Biology and Molecular Medicine at Yenepoya (Deemed to be University) under the Biotechnology Skill Enhancement Program in Multiomics Technology (BiSEP GO ITD 02 MDA 2017).

Author contributions
P. K. M. and T.S.K.P. conceived the idea, designed the experiments and interpretation of data, and critically reviewed and edited the manuscript. S. A. performed experiments and data analysis, drafted the manuscript, and prepared figures. R.P. conceptualized the study and interpretation of data. C. S. A. performed docking experiments and drafted the manuscript. S.S. U. drafted the revised manuscript, prepared the figure; all authors read and approved the final version of the manuscript.

Declaration

Competing interests
The authors declare no competing interests.

Consent for Publication
All authors have read and approved the manuscript and consent to its publication.

Additional information
Supplementary Information The online version contains supplementary material available at https://doi.org/10.1038/s41598-025-92756-5.

Correspondence and requests for materials should be addressed to T.S.K.P. or P.K.M.